Virus Transport under Transient Flow Conditions

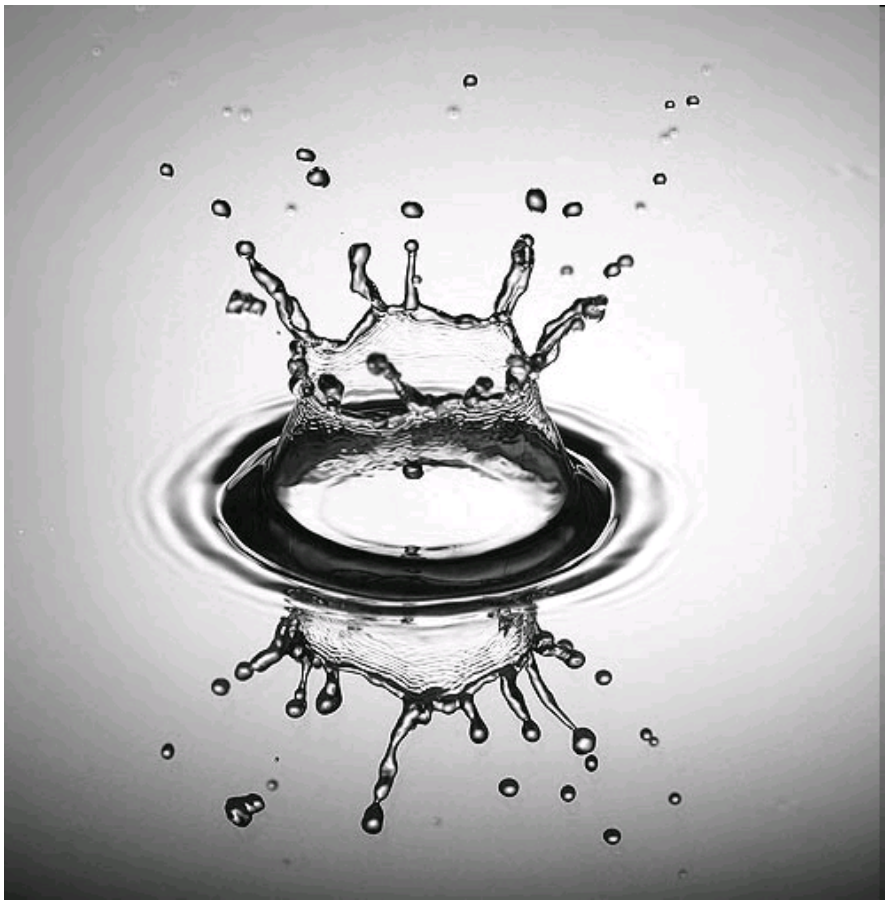

Saskia Maria Roels

MSc Thesis Hydrogeology
Department of Earth Sciences
Utrecht University

Virus Transport under Transient Flow Conditions

21 October 2009

Supervisors:

Prof. dr. ir. S. Majid Hassanizadeh
Professor of Hydrogeology
Department of Earth Sciences
Faculty of Geosciences
Utrecht University, The Netherlands

Dr. Jack F. Schijven
Expert Centre for Methodology and Information Services
National Institute of Public Health and the Environment (RIVM)
Bilthoven, The Netherlands

Drs. Amir Raoof
Department of Earth Sciences
Faculty of Geosciences
Utrecht University, The Netherlands

Saskia Maria Roels 0340685
saskiaroels@hotmail.com

MSc Thesis Hydrogeology
Department of Earth Sciences
Utrecht University

Foreword

First of all, I would like to express that I really enjoyed working on this research. It was an experience in which I have learned as much about hydrogeology as my own personality. To be alone with your computer for almost one year, without any strict deadline and a lot of time to think, revealed to me that everything is possible, as long as you are dedicated to what you are doing.

I would like to thank my supervisor and coordinator Majid Hassanizadeh, who has learned me so much. He really got me interested in science and gave me the self confidence to complete this research successfully. Also, I would like to thank Jack Schijven, who was always prepared to visit university and enthusiastically explain detailed information about the behavior of viruses. Of course I am also thankful to Amir for his support when my computer and I were failing.

I would also like to thank my parents, Guus Roels and Bibi Karstel, for their support throughout my study. They have always encouraged me to develop my ambitions and interests. My sister, cousins and friends, thank you all for showing interest in the crazy world of science. Also my classmates and other students with whom I have shared the office last year, thanks for your support.

Summary

Riverbank filtration (RBF) is a potential and low-cost technology that provides cleaner and safer water for agriculture and pre-treated water for human consumption. In RBF, water from rivers or lakes is forced to pass through the river bank flow towards extraction wells placed sufficiently close to the surface water body. Through urban and agricultural activities, pathogenic microorganisms (viruses, bacteria and parasitic protozoa) can enter the aqueous environment and can endanger public health. By RBF, filtration processes can effectively remove pathogenic microorganisms from the water.

However, recent studies have shown that the efficiency of removal of pathogenic microorganisms from groundwater depends highly on hydrological and geochemical factors that may vary widely spatially and temporally. Column experiments have shown an increase in virus concentration at the outlet with the arrival of a drying front during drainage (Torkzaban et al., 2006a Powelson and Mills, 2001; Saiers et al., 2003) or a wetting front during imbibition (Sirivithayapakorn and Keller, 2003; Shang et al., 2008; Sharma et al., 2008). This means that the foreseen climate changes with more frequent periods of heavy rainfall throughout the year and therefore varying water tables, can lead to peak concentrations in drinking water generated by RBF. Such peak events are of major importance to public health risk (Westrell et al., 2006).
This research aimed to provide a better understanding of the remobilization processes of small particles (e.g. colloids, bacteria and viruses) and predict the fate and behavior of virus particles in soil columns. The research consists of two parts: one review on attachment and detachment mechanisms at interface and pore scale and one model of a virus transport experiment. The model was based on a drainage experiment done by Torkzaban et al. (2006).

Detachment of a particle from a solid surface during drainage or imbibition was found to be caused by surface tension detachment forces as a result of interfacial tension between air and water. Theoretical calculations have shown that surface tension forces are generally much higher than adhesion forces (Gómez-Suárez et al., 2001b). The appearance of a strong surface tension detachment force as a result of particle and air-water interface (AWI) collision during drainage can sweep the particle from the solid surface. During imbibition, the initially attractive surface tension force can become repulsive at a certain filling angle through which the particle can be removed from the solid surface. These mechanisms may lead to a peak concentration in the groundwater.
Virus transport in the soil column was modeled by two concepts and compared. One concept treats the detachment rate as a constant that increases when a transient flow condition is applied. The other concept is a variable detachment rate that depends on change in water content, proposed by Cheng and Saiers (2009). Comparison of the models with respect to the experimental data of Torkzaban et al. (2006) showed that the concept of Cheng and Saiers (2009) could fit the data reasonably well and significantly better than the concept of the constant detachment rate. Because not every situation can be evaluated by measuring virus removal from groundwater, a model that reliably predicts removal over a certain time or distance is very useful for RBF.

Background

Riverbank filtration (RBF) is a recently developed low-cost technology that provides cleaner and safer water for agriculture and pretreated water for human consumption. Water from rivers or lakes is subjected to subsurface flow towards extraction wells placed sufficiently close to the surface water body. From land application of raw and treated wastewater, septic wells, effluent from septic tanks, leaking sewage pipes, and animal manure (Gerba and Smith, 2005), (emerging) pathogenic microorganisms are introduced into the aqueous environment. During subsurface flow microorganism concentrations have the potential to decrease due to dilution, adsorption and inactivation (Weiss et al., 2003). Pathogens still present in drinking water, even at concentrations below detection limit, may be ingested and lead to illness. To obtain insight in optimal distances between a surface water body and extraction wells, modeling of virus transport through the subsurface is required.

The efficacy of RBF treatment strongly depends on hydrological and geochemical factors that may vary widely spatially and temporally. Several studies have been done on the effects of the degree of water saturation, flow rate, pH, hydrophobicity and electrostatic and capillary forces on the removal of viruses from water (e.g. Saiers et al., 2003; Torkzaban et al., 2006a/b; Shang et al., 2008; Powelson and Mills, 2001; El-Farhan et al., 2000; Kaplan et al., 1993; Ryan et al., 1998). It was found that water content plays a significant role in virus removal (Chu et al., 2001; Jin et al., 2000; Lance and Gerba, 1984; Powelson et al., 1990; Poletika et al., 1995). In a steady state flow situation, a lower water content leads to more retention of viruses due to enhanced adsorption to the soil-water interface (SWI) and air-water interface (AWI) (Torkzaban et al., 2006a).

However, in the vadose zone, variable saturation degrees and transient-flow regimes are present which are triggered by variations in, for example, precipitation, transpiration and water table fluctuations. It has been shown that detachment rates of colloids from soil grains subject to temporal variability in moisture content and pore water velocity are higher than detachment rates under steady-flow conditions (Kaplan et al., 1993; Ryan et al., 1998; El-Farhan et al., 2000). In addition, the colloid detachment rates vary over the course of imbibition and drainage, e.g. wetting and drying fronts (Ryan et al., 1998). Several column experiments (Powelson and Mills, 2001; Saiers et al., 2003; Cheng and Saiers (2009); Torkzaban et al., 2006b) showed a sudden rise in concentrations at the end of the breakthrough curves when the columns were drained. The increase in concentration at the outlet was observed with the arrival of a drying front during drainage (Torkzaban et al., 2006; Powelson and Mills, 2001; Saiers et al., 2003) or a wetting front during imbibition (Sirivithayapakorn and Keller, 2003; Shang et al., 2008; Sharma et al., 2008). Due to the advancing soil-water-air contact line during drainage, cells adsorbed to the solid grains can be dislodged, causing an increase in the breakthrough concentration. It was hypothesized that the net effect of adsorption to increased AWI's and sweeping from the solid surface by SWA contact line may depend on the frequency of changes in water content, where a higher frequency dominates the sweeping process (Powelson and Mills, 2001). Also imbibition studies have indicated that particles can be remobilized during resaturation (e.g. Chen and Flury, 2005; Crist et al., 2001; Saiers and Lenhart,

2003; Gao et al., 2006). Colloid breakthrough curves of imbibition experiments show a steep breakthrough and a long elution tail (Shang et al., 2008; Saiers and Lenhart, 2003). The long-lasting tails indicate kinetic-controlled colloid release.

Remobilization of previously deposited pathogenic microorganisms can lead to peak concentrations in drinking water generated by RBF. Such peak events are of major importance to public health risk (Westrell et al., 2006). In this regard, waterborne pathogenic viruses are of major concern, because of their persistence in the aqueous environment, their infectivity and their ability to be transported in with groundwater. Dutch drinking water legislation (VROM, 2001) requires that the concentrations in drinking water of the so-called index pathogens of enteroviruses, *Campylobacter*, *Cryptosporidium* and *Gardia* are low enough to comply with a maximum risk of infection of 10^{-4} person per year from drinking from drinking water consumption. According to foreseen climate changes, periods of heavy rainfall are more frequent throughout the year, also in the Netherlands, with more frequent events of flooding, therefore such peak concentrations of pathogens in abstracted water are expected to occur more frequently (Schijven and de Roda Husman, 2005).

This research aimed to provide a better understanding of virus transport mechanisms and to optimize modeling estimations of virus concentration in water under transient flow regimes. The first part of this research focuses on the forces involved in attachment and detachment of particles during transport in water. To understand the processes that cause additional detachment during drainage and imbibition, an overview is given of attachment and detachment mechanisms on interface and pore scale. The second part of this research consists of a model of a drainage experiment. The model accounts for variable water content dependent detachment and can, therefore, more reliably predict virus concentrations than a steady state model.

References

Chen, G., and M. Flury (2005) Retention of mineral colloids in unsaturated porous media as related to their surface properties. Colloids Surf. A. 256:207– 216

Cheng, T and Saiers S E (2009) Mobilization and transport of in situ colloids during drainage and imbibition of partially saturated sediments. Water Resources Research Vol 45, W08414, doi:10.1029/2008WR007494, 2009

Chu, Y., Y. Jin, M. Flury, M.V. Yates (2001) Mechanisms of virus removal during transport in unsaturated porous media. Water Resources Research Vol. 37, NO. 2:253-263

Crist, J. T., Y. Zevi, J. F. McCarthy, J. A. Troop, T.S. Steenhuis (2005) Transport and retention mechanisms of colloids in partially saturated porous media, Vadose Zone J. 4:184–195

El-Farhan, Y. H., N.M. Denovio, J.S. Herman, G.M. Hornberger (2000) Mobilization and transport of soil particles during infiltration experiments in an agricultural field. Shenandoah Valley, Virginia, Environ. Sci. Technol. 34:3555– 3559

Gao, B., J. E. Saiers, J. N. Ryan (2006) Pore-scale mechanisms of colloid deposition and mobilization during steady and transient flow through unsaturated granular media. Water Resour. Res. 42, W01410, doi:10.1029/2005WR004233

Gerba, C.P., and J.E. Jr. Smith (2005) Sources of pathogenic microorganisms and their fate during land application of wastes. J. Environ. Qual. 34:42–48

Gómez-Suárez, C., H.J. Busscher, H.C. van der Mei (2001b) Analysis of Bacterial Detachment from Substratum Surfaces by the Passage of Air-Liquid Interfaces. Appl. and Envir. Microbiology 2531-2537

Jin, Y., Y.Chu, Y. Li (2000) Virus removal and transport in saturated and unsaturated sand columns. J. Contam. Hydrol. 43:111 –128

Kaplan, D. I., P.M. Bertsch, D.C. Adriano, W.P. Miller (1993) Soil-borne mobile colloids as influenced by water flow and organic carbon, Environ. Sci. Technol. 27:1193– 1200

Lance, J. C. and C.P. Gerba (1984) Virus movement in soil during saturated and unsaturated flow. Appl. Environ. Microbiol. 47:335– 341

Poletika, N. N., W.A. Jury, M.V. Yates (1995) Transport of bromide, simazine, and MS-2 coliphage in a lysimeter containing undisturbed, unsaturated soil. Water Resour. Res. 31:801–810

Powelson, D. K., J.R. Simpson, C.P. Gerba (1990) Virus transport and survival in saturated and unsaturated flow through soil columns. J. Environ. Qual. 19:396–401

Powelson, D. K., A.L. Mills (2001) Transport of Escherichia in Sand Columns with Constant and Changing Water Contents. J. Environ. Qual. 30:238-245

Ryan J.N., T.H. Illangasekare, M.I. Litaor, R. Shannon (1998) Particle and plutonium mobilization in macroporous soil during rainfall simulations. Environ. Sci. Technol. 32: 476– 482

Saiers, J.E., G.M. Hornberger, D.B. Gower, J.S. Herman (2003) The role of moving air-water interfaces in colloid mobilization within the vadose zone. Geophys. Res. Lett. 30, No 21

Saiers, J. E., and J. J. Lenhart (2003) Colloid mobilization and transport within unsaturated porous media under transient-flow conditions. Water Resour. Res. 39(1), 1019, doi:10.1029/2002WR001370

Schijven, J.F., A.M. de Roda Husman (2005) Effect of climate changes on waterborne disease in The Netherlands. Water Sci Technol. 2005;51(5):79-87

Shang, J., M. Flury, G. Chen, J. Zhuang (2008) Impact of flow rate, water content, and capillary forces on in situ colloid mobilization during infiltration in unsaturated sediments. Water Resour. Res. 44

Sharma, P., M. Flury, J. Zhou (2008) Detachment of colloids from a solid surface by a moving air-water interface. Journal of Colloid and Interface Science 326:143-150

Sirivithayapakorn, S., and A. Keller (2003) Transport of colloids in unsaturated porous media: a pore-scale observation of processes during the dissolution of the air-water interface. *Water Resour. Res.*, *39*, 1346, doi: 10.1029/2003WR002487
Torkzaban, S., S.M. Hassanizadeh, J.F. Schijven, A.M. de Bruin, A.M. de Roda Husman (2006a) Virus Transport in Saturated and Unsaturated Sand Columns. Vadose Zone Journals 5:877-885
Torkzaban, S., S.M. Hassanizadeh, J.F. Schijven, H.H.J.L. van den Berg (2006b) Role of air-water interfaces on retention of viruses under unsaturated conditions. Water Resources Research Vol 42, W12S14, doi:10.1029/2006WR004904
Weiss, W.J., E.J. Bouwer, W.P. Ball, C.R. O'Melia, H. Aurora, R. Aboytes, T.F. Speth (2003) Study of water quality improvements during riverbank filtration at three midwestern United States drinking water utilities. EGS - AGU - EUG Joint Assembly, Abstracts from the meeting held in Nice, France, 6 - 11 April 2003
Westrell T., P. Teunis, H van den Berg, W. Lodder, H. Ketelaars, T.A. Stenström, A.M. de Roda Husman (2006) Short- and long-term variations of norovirus concentrations in the Meuse river during a 2-year study period. Water Res 2006, 40, 2613-2620.

Part 1: Review

Supervisors:

Prof. dr. ir. S. Majid Hassanizadeh
Professor of Hydrogeology
Department of Earth Sciences
Faculty of Geosciences
Utrecht University, The Netherlands

Dr. Jack F. Schijven
Expert Centre for Methodology and Information Services
National Institute of Public Health and the Environment (RIVM)
Bilthoven, The Netherlands

Table of Contents

Introduction

As was found in previous research, virus transport in (ground)water is significantly influenced by changes in water content. In order to understand the mechanisms involved in virus transport under transient flow conditions, the first part of this research aims to give a summary of the detachment mechanisms of viruses, bacteria and colloids at interface and pore scale.

On aquifer scale or column scale, the differences in transport processes between colloids, bacteria and viruses is mostly observed in dissimilarities in retention processes. Because of their relatively large size, colloid and bacteria retention is also caused by straining (Bradford et al., 2002), whereas virus and bacteria removal is affected by inactivation (Keswick and Gerba, 1980; Yates et al., 1987). However, this paper focuses more on interface scale. Various forces play a role in detachment and attachment of colloids, bacteria and viruses, which are discussed in detail in this paper. Differences in particle size and hydrophobicity can lead to stronger or weaker forces, but the concept of relevant forces is the similar for all particles. Unless a specific example is given from a previous research, colloids, bacteria and viruses are all referred to as ‘particles’.

In the first chapter, attachment mechanisms under saturated conditions are discussed. A theoretical overview is given about the favourable attachment locations in a saturated pore and how different forces are acting on an attached particle. The second chapter treats similar attachment mechanisms under unsaturated conditions. The effect of drainage and imbibition events on particle detachment is discussed in chapter three. Chapters four and five describe results from drainage and imbibition experiments, respectively, done in previous researches. The results are discussed and compared to the theoretical concepts of attachment and detachment processes.

1. Particle Attachment under Saturated Conditions

1.1. Locations of Particle Attachment

Spreading of particles in subsurface water is affected by advection and dispersion (Schijven and Hassanizadeh; 2000). During soil passage particles can be removed from saturated flow by attachment to solid grains. Figure 1 presents a simplification of pore geometry as a triangular cross section in which the velocity distribution is considered (Bradford and Torkzaban, 2008). Favorable locations for colloid retention are the low velocity regions in the corners of the pore space.

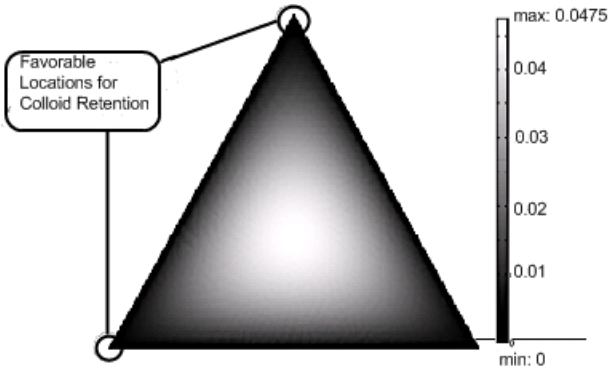

Fig. 1. The velocity distribution in a saturated triangular capillary tube with average pore water velocity of 0.02 m d^{-1} (Bradford and Torkzaban, 2008)

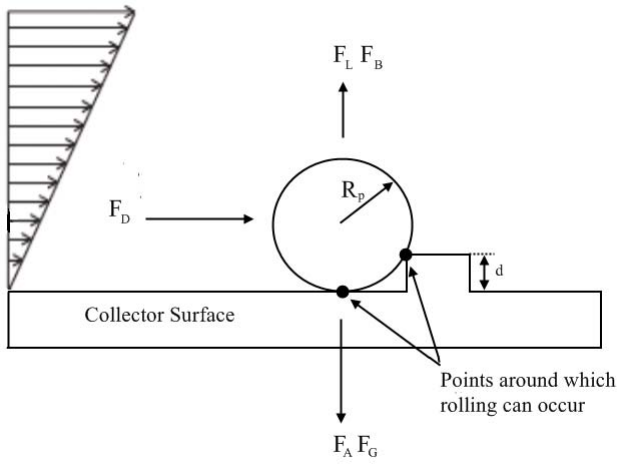

Fig. 2. Schematic of an adhering particle and the relevant forces acting on it in a moving fluid. The surface roughness is denoted as d. (Burdick et al., 2005; Veerapaneni et al., 2000)

At interface scale, several forces are acting on an attached particle depending on grain surface and particle properties (Figure 2). A balance between an adhesion force, F_A, gravity force, F_G, drag force, F_D, buoyancy force, F_B, and lift force, F_L, determines whether the particle remains attached to or will be detached from the solid grain. The next two sections describe the adhesion force, drag force and lift force in detail. The gravity and buoyancy forces are considered to be negligible, because of the small size of the particles considered in this research, and will not be discussed.

1.2. Adhesion Force

The adhesion force, F_A, normally works perpendicular to the solid grain surface and adheres the particle to the surface. F_A is generally calculated by the classical or extended DLVO theory through a combination of Lifshitz-van der Waals forces, Φ^{vdW}, attractive or repulsive electrostatic interactions,Φ^{edl}, and additional hydrophobic or acid-base forces (Sharma et al., 2005; Grasso et al., 2002). The total potential energy, Φ^{tot} [ML^2T^{-2}], through interactions of colloids approaching each other or the AWI and SWI was evaluated as a function of the separation distance, x (Derjaguin and Landau, 1941; Verwey and Overbeek, 1948):

$$\Phi^{tot}(x) = \Phi^{vdW}(x) + \Phi^{edl}(x) + \Phi^{add}(x) \quad (1)$$

where Φ^{add} [ML^2T^{-2}] represents the additional forces which are especially considered for interactions of colloids with the AWI and of hydrophobic colloids with each other. This term could represent all kinds of non-DLVO interactions that may occur under particular circumstances, including H bonding, hydrophobic interactions, hydration pressure, non-charge-transfer Lewis acid-base interactions, and steric interactions (Grasso et al., 2002).

The van der Waals potential for the unretarded sphere-sphere interaction was estimated using Eq. (2) (Hamaker, 1937) and colloid interaction with a macroscopic flat surface was approximated by Eq. (3) (Norde and Lyklema, 1989):

$$\Phi^{vdW} = -\frac{A_{123}}{12}\left\{\frac{y}{r^2+ry+r} + \frac{y}{r^2+ry+r+y} + 2\ln\left(\frac{r^2+ry+r}{r^2+ry+r+y}\right)\right\} \quad (2)$$

$$\Phi^{vdW} = -\frac{A_{123}}{6}\left\{\frac{2R_p(x+R_p)}{x(x+R_p)} - \ln\left(\frac{x+R_p}{x}\right)\right\} \quad (3)$$

where $y = R_g/R_p$, $r = x/R_p$, and R_p and R_g are the particle and grain radii [L], respectively; x [L] is the separation distance; and A_{123} [$M\,L^2\,T^{-2}$] is the complex Hamaker constant which is typically estimated from the following expression (Israelachvili, 1992):

$$A_{123} = \left(\sqrt{A_{11}} - \sqrt{A_{33}}\right)\left(\sqrt{A_{22}} - \sqrt{A_{33}}\right) \quad (4)$$

where A_{11}, A_{22} and A_{33} [$M\,L^2\,T^{-2}$] are the Hamaker constants for each component.
The electrostatic double layer interactions can be determined using the constant surface potential interaction expression of Hogg et al. (1996) for a sphere-sphere interaction (Eq. (5)) and the Norde and Lyklema (1989) expression for interaction of colloids with the sand grains or the AWI (Eq. (6)):

$$\Phi^{edl} = \frac{\pi\varepsilon\varepsilon_0 2R_p}{2R_p + R_g}\left\{2\Psi_{0c}^2 \ln\left(\frac{1+\exp(-\kappa x)}{1-\exp(-\kappa x)}\right) + \left(2\Psi_{0c}^2\right)\ln\left[1-\exp(-2\kappa x)\right]\right\} \quad (5)$$

$$\Phi^{edl} = \pi\varepsilon\varepsilon_0 R_p \left(\Psi_{0c}^2 \Psi_{0s}^2\right)\left\{\frac{2\Psi_{0c}\Psi_{0s}}{\Psi_{0c}^2\Psi_{0s}^2}\ln\left[\frac{1+\exp(-\kappa x)}{1-\exp(-\kappa x)}\right]+\ln\left[1-\exp(-2\kappa x)\right]\right\} \qquad (6)$$

where ε [-] is the dielectric constant of water, ε_0 [$M^{-1}L^{-3}T^4A^{-2}$, where A denotes ampere] is the permittivity of free space, Ψ_{0c} [$M\ L^2\ T^{-3}A^{-1}$] is the surface potential of the colloid, Ψ_{0s} [$M\ L^2\ T^{-3}A^{-1}$] is the surface potential of the flat surface, and κ [L^{-1}] is the reciprocal double layer thickness calculated from the valence and the ionic strength of the electrolyte solution.

With respect to hydrophobic interactions between a colloid and a collector surface, the hydrophobic interaction energy can be included in the last term of Eq. (1), which becomes $\Phi^{hyd}(x)$ and can be expressed as (Schäfer et al., 1998):

$$\Phi^{hyd}(x) = -\frac{K_{123}R_p}{x} \qquad (7)$$

where K_{123} [ML^2T^{-2}] is the force constant for the asymmetric interactions between macroscopic bodies 1 and 2 in medium 3. The value of K_{123} has been determined as (Yoon et al., 1997; Schäfer et al., 1998):

$$\log K_{123} = a\left(\frac{\cos\theta_c + \cos\theta_2}{2}\right)+b \qquad (8)$$

where θ_c [º] is the air-water contact angle on a particle surface, and θ_2 [º] is the air-water contact angle on the second surface (collector surface), and *a* and *b* are system-specific constants. To analyze the behavior of Eq. (7) and (8), consider a contact angle of 180º for the AWI, (Schäfer et al., 1998) and system-specific constants of a= -6 and b = -22 (both dimensionless) (Crist et al., 2005). Two bacterial strains with similar radii and different hydrophobicities are listed in Table 1. If the contact angles are applied to Eq. (7) and (8), it is found that the hydrophobic *attractive* interaction energy of the more hydrophilic bacterial strain, *S. oralis* J22, with the AWI is lower than the hydrophobic *attractive* interaction energy of the less hydrophilic bacterial strain, *A. naeslundii* T14V-J1, at a separation distance of 2 nm.

Table 1. Bacterial Properties

Bacteria	**Radius (R_p, nm)**	**Water Contact Angle (°)**	**Φ^{hyd} (kg m^2 s^{-2})**
S. oralis J22	± 500	24	-4.54×10^{-20}
A. naeslundii T14V-J1	± 500	64	-1.21×10^{-18}

An example of calculated DLVO interaction energies between a given particle and a collector surface is shown in Figure 3. The total interaction energy varies with ionic strength, colloid size, zeta-potential of the particle and zeta-potential of the solid surface.

In these calculations extra terms were added to account for hydrophobic interactions and Born repulsion. In Figure 3, a primary and a secondary energy minimum are present. It was found that the secondary minimum increases with particle size and ionic strength (Bradford and Torkzaban, 2008). Therefore, due to their relatively small size, the secondary minimum could be absent for viruses. Due to a high energy barrier between the primary and secondary minimum, it is most likely that a particle will attach in the secondary interaction minimum. Also, in the situation as shown in Figure 3, no energy is required for a particle to get into the secondary minimum. Other DLVO calculations revealed a total absence of a primary minimum on glass (Boks et al., 2008).

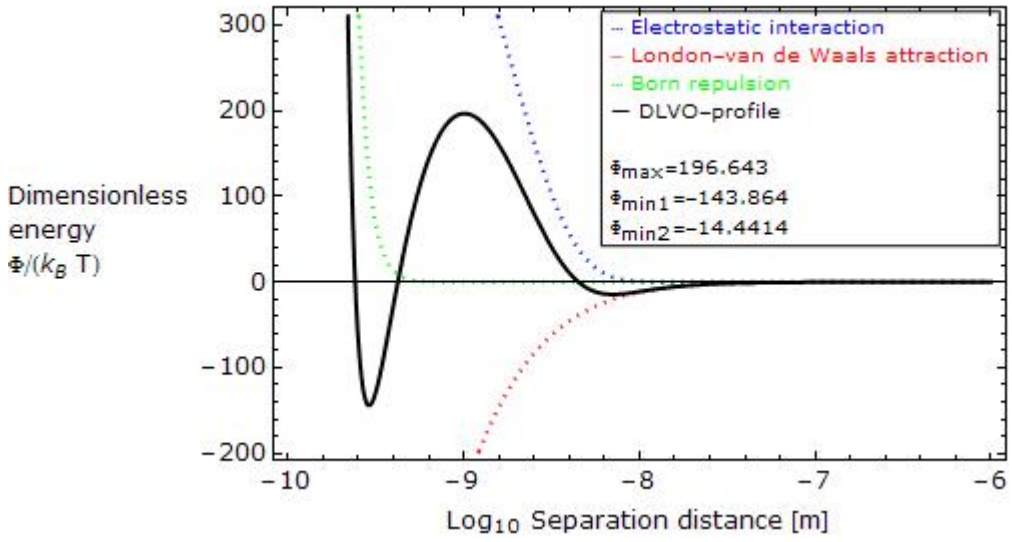

Fig. 3. Interfacial potential energies for colloids as a function of separation distance to the grain surface. Ionic strength is 0.05 M, colloid size is 10^-6 m, zeta-potential of the particle is -20 mV and zeta-potential of the solid surface is -25mV.

To calculate the adhesive force, F_A, from the DLVO interaction energy, the Derjaguin and Langbein approximation can be used (Isrealachvili, 1992):

$$F_A = \frac{\Phi_{\min}}{x} \qquad (9)$$

where Φ_{min} [ML^2T^{-2}] is the absolute value of the secondary or primary minimum interaction energy. Exploration of Eq. (3), (6) and (9) indicates that the strength of the adhesion force depends upon the particle size, with stronger adhesion forces for larger particles.

1.3. Drag and Lift Forces

Drag forces, F_D, and lift forces, F_L, can oppose the effect of adhesion forces and may cause detachment of a particle from a solid grain. For laminar flow, the lift force can be estimated with the following correlation (Bergendahl and Grasso, 2000):

$$F_L = \frac{81.2\mu R_p^3 \left(\frac{\partial V}{\partial r}\right)^{3/2}}{v^{1/2}} \qquad (10)$$

where $\delta V/\delta r$ [T^{-1}] is the hydrodynamic shear at a distance of R_p [L] from the surface, μ [$ML^{-1}T^{-1}$] is the fluid dynamic viscosity and ν [L^2T^{-1}] is the fluid kinematic viscosity. However, when the flow is laminar, lift forces that act perpendicular to the surface are generally considered negligible because of their weakness (Soltani and Ahmadi, 1994; Sharma et al., 2005).

The drag force acting on a particle can be calculated using the following equation (Goldman et al., 1967; O'Neill, 1968):

$$F_D = 10.205\pi\mu\left(\frac{\partial V}{\partial r}\right)R_p^2 \qquad (11)$$

When the drag force reaches a critical limit and exceeds the adhesion force (Liu and Tay, 2002), particles can be detached from a collector surface. Detachment of a particle can occur through lifting, sliding and rolling (Burdick et al., 2005). Under laminar flow conditions, the latter is considered of greatest importance (Soltani and Ahmadi, 1994; Bergendahl and Grasso, 1998, 1999, 2000). Depending on the surface roughness, δ_l, (Figure 2), rolling can occur at different points.

Results from an experiment with different collector surfaces and bacterial strings (Boks et al., 2008), show that detachment due to drag forces also depends upon surface hydrophobicity. Six types of hydrophilic bacterial strains were examined on their detachment behavior from hydrophilic and hydrophobic collector surfaces under increasing drag forces. In most cases, the bacteria were more readily detached by drag forces from the hydrophilic surface than from the hydrophobic surface.

A similar research with different bacteria hydrophobicities and a hydrophilic glass plate surface was done by Sharma et al. (2005). The fluid shear alone could effectively detach the more hydrophilic bacterial strains from the hydrophilic collector surface, but not the more hydrophobic bacterial strains. According to Eq. (11) both the hydrophilic and hydrophobic bacterial strains experience the same drag force. Differences in detachment, therefore, could be found in different DLVO interaction energy patterns.

2. Particle Attachment under Unsaturated Conditions

2.1. Locations of Particle Attachment

It has been shown in several studies that virus removal from water under steady state conditions increases with smaller water content (Torkzaban et al., 2006; Chu et al., 2001; Keller and Sirivithayapakorn, 2004; Powelson and Mills, 2001; Thompson and Yates, 1999). Different explanations are given for this phenomenon. Keller and Sirivithayapakorn (2004) found an increase in retention at AWI's and straining in thin-water films. According to Torkzaban et al. (2006a) diffusion lengths decrease as a result of decreasing water content which leads to faster adsorption kinetics at the solid grains. Attachment to AWI's was considered to be less important in their research. The same result was observed in a study done by Chu et al. (2001) in which the amount of reactive solid surfaces, i.e. the amount of surfaces with favorable attachment conditions, varied. Virus removal from subsurface water under unsaturated conditions depended upon available reactive solid surfaces rather than available AWI's. This indicated that attachment to the SWI was the main retention mechanism. However, removal from the water could also be virus dependent as was seen by Thompson and Yates (1999). In their batch experiments bacteriophages MS2 and R17 did attach to the AWI and SWA contact line, whereas φX174 did not significantly. In a previous study (Thompson et al., 1998), it was already found that inactivation predominantly takes place at the SWA contact line. The more AWI's and hydrophobic SWA contact lines were available, the higher the inactivation of MS2 and R17 was. This indicated that the AWI's and SWA contact lines were favorable attachment sites for MS2 and R17. It was suggested that φX174, because of its dominant hydrophilicity, did not readily accumulate at AWI's and SWA contact lines, while the more hydrophobic MS2 and R17 did.

Altogether, based on these researches, it can be stated that particles can be attached in an unsaturated pore at different locations (Figure 4). Location 1 represents attachment to the SWI, Location 2 represent attachment to the AWI, and Location 5 represent attachment to the SWA contact line. Attachment of a particle at two bounding SWI's (Location 3) has been referred to as wedging (Johnson et al., 2007) or straining (Bradford et al., 2006a/b). It was already mentioned that these processes strongly depend upon particle size. At Location 4 multiple particles collide, which has been called bridging (Ramachandran and Fogler, 1999) or straining (Bradford et al., 2002). Location 6 shows film straining, as was observed in the study by Keller and Sirivithayapakorn (2004). Also straining in immobile water zones could be an important particle retention mechanism (Gao et al., 2006). In this paper, retention in immobile water zones is represented in Locations 7.

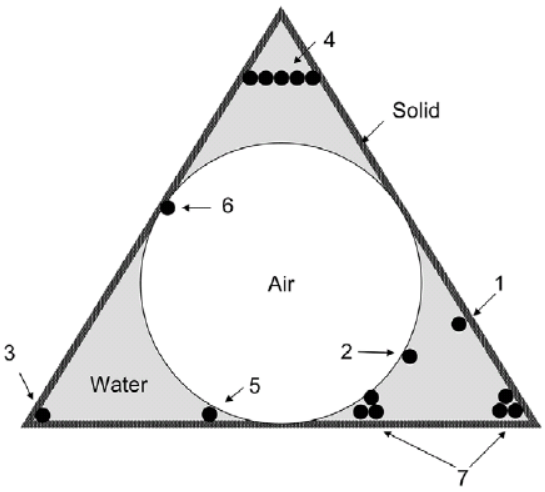

Fig.4. A schematic of the various pore-scale colloid retention processes. Colloid retention at Locations 1 and 2 occurs via attachment to the SWI and AWI, respectively. Colloid retention at Locations 3, 4, 5, and 6 occurs via various straining mechanisms, namely: 3, wedging; 4, bridging; 5, retention at the SWA; and 6, film straining. Location 7 indicates straining in immobile water regions (Bradford and Torkzaban., 2008)

In Chapter 1, the relevant forces that act on a particle attached to the SWI have been discussed. DLVO forces between particle and SWI and between two particles are the main retention mechanisms at Locations 1, 3 and 4. A particle retained by the AWI (Location 2), by film straining (Location 6) or by the SWA contact line (location 5) experiences both capillary forces and DLVO forces (Chen and Flury, 2005; Shang et al., 2008). It was found that capillary forces dominate DLVO forces and is therefore at these locations the main force that retains the particle (Shang et al., 2008).

2.2. Capillary Force

The capillary force between a spherical colloid and a grain surface (Locations 5 and 6) (Chateau et al., 2002) as well as between a spherical colloid and the AWI (Locations 2 and 5) (Zhang et al., 1996; Veerapaneni et al., 2000) can be calculated by (see Figure 5):

$$F_{cap} = 2\pi R_p \gamma_{lv} \sin\phi \sin(\theta - \phi) - \Delta p \pi R_p^2 \sin^2\phi \qquad (12)$$

where R_p [L] is the radius of the colloid; γ_{lv} [MLT^{-2}] is the air-water interfacial tension; φ [°] is the filling angle between the center of the colloidal sphere and the water-colloid contact line; θ [°] is the colloid water contact angle and Δp is the capillary pressure defined as the pressure jump across the AWI. The first time on the right hand side is often referred to as surface tension force and the second term as pressure force. Note that a negative capillary force represents an attractive force.

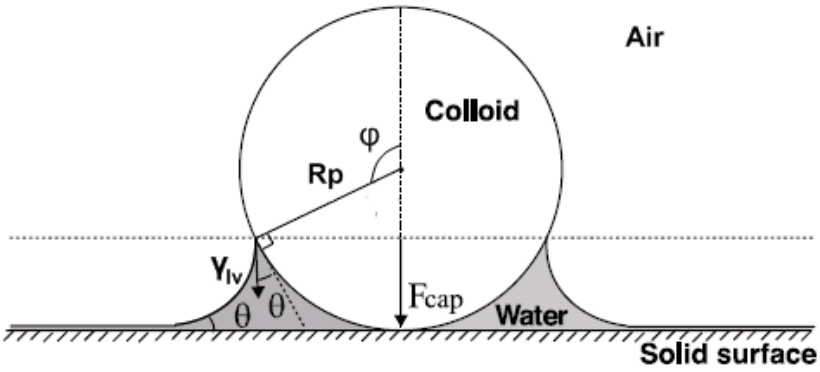

Fig. 5. Schematic of a spherical colloid in contact with a flat sediment surface in a water film (Shang et al., 2008)

A particle that is attached to the AWI by capillary forces (Eq. (12)) may actually penetrate the AWI. The penetration distance, D_0, can be estimated according to Ducker et al. (1994) as follows:

$$D_0 = R_p(1-\cos\beta) \tag{13}$$

where β [º] is the contact angle between the particle and the AWI.

3. Particle Detachment during Drainage and Imbibition Events

3.1. Surface Tension Force

As mentioned in the background, under changing water contents additional particles can be removed from solid surfaces. These particles could be attached under saturated conditions (Figure 1) or under unsaturated conditions (Figure 4).

In Figure 6, F_γ represents the surface tension force as already shown in the in first term on the right hand side of Eq. (12). The surface tension force is the resultant of occurring interfacial tension between water and air during two phase flow. According to the filling angle, φ, the surface tension force can either be attractive or repulsive. Detachment can occur when the repulsive surface tension force exceeds the adhesion force between a colloid and a collector surface. The theoretical surface tension detachment force can be given by (Figure 6; Leenaars and O'Brien, 1989):

$$F_\gamma = 2\pi R_p \gamma_{lv} \sin\left[\phi(t)\right] \sin\left[\theta - \phi(t)\right] \qquad (14)$$

where R_p [L] is the radius of the particle; γ_{lv} [MLT^{-2}] is the air-water interfacial tension; φ [º] is the filling angle between the center of the colloidal sphere and the water-colloid contact line; and θ [º] is the contact angle between the surface of the particle and the AWI.

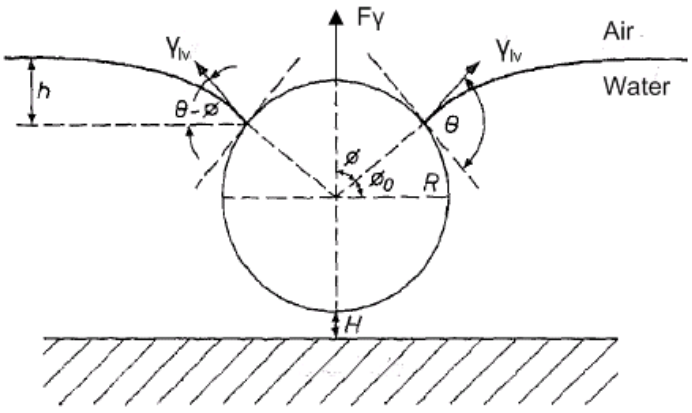

Fig. 6. Removal of a particle from a horizontal substrate (theoretical procedure). Snap-shot during drainage or imbibition at which detachment takes place.

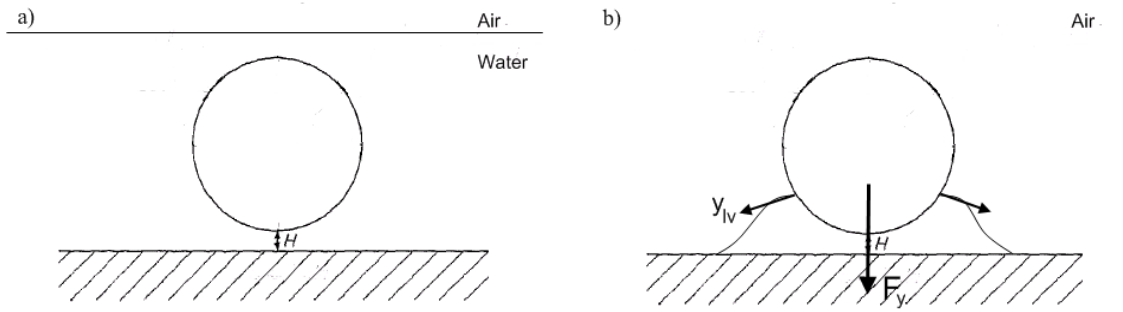

Fig. 7. a) Attached particle under saturated conditions; b) Attached particle under unsaturated conditions.

In Figure 7a, a particle attached under saturated conditions is shown and Figure 7b represents a particle attached under unsaturated conditions. During drainage, the water level in Figure 7a will drop and during imbibition the water level in Figure 7b will rise. For the drainage scenario it means that the surface tension force starts to act on the particle as soon as the AWI collides with the particle. During unsaturated attachment, it was already shown that the surface tension force attaches the particle to the surface at low water content (Figure 5, Eq. (12)). However, as the water level rises, the attractive surface tension force becomes repulsive and can cause detachment. A repulsive surface tension force is often referred to as surface tension detachment force.

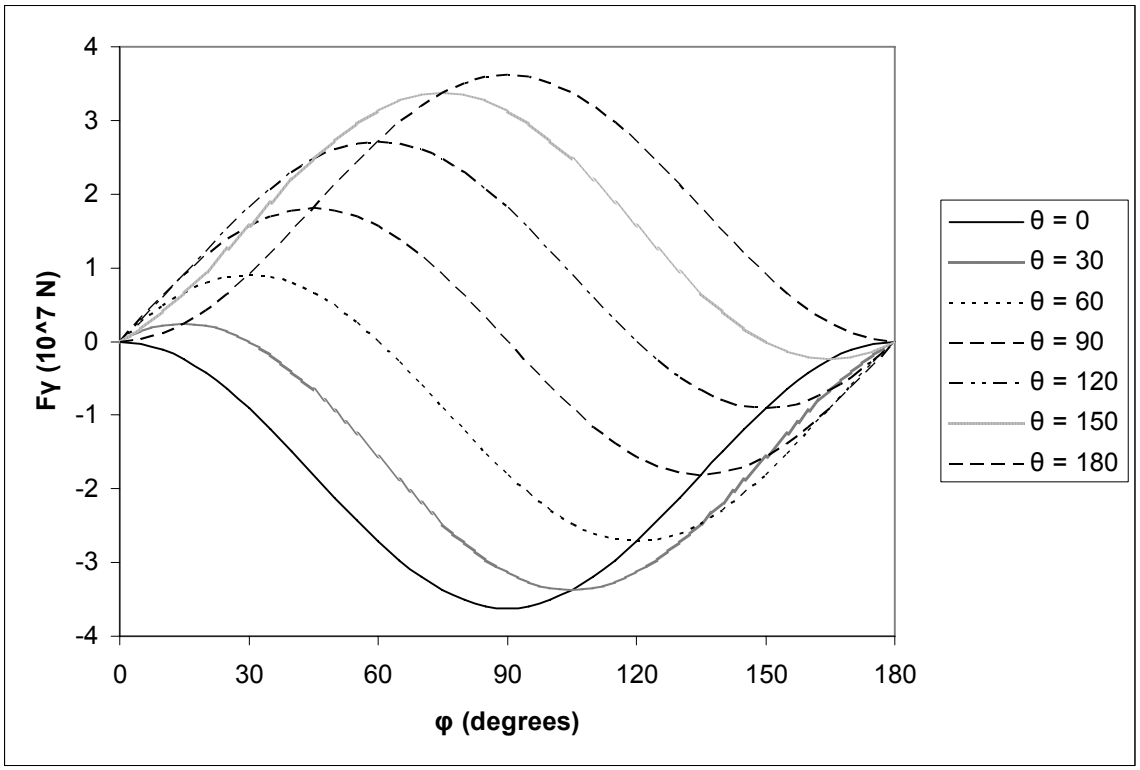

Fig.8. Theoretically calculated surface tension forces from Eq. (16) for different values of θ and φ and for a bacterium with an R_p of 800 nm and a γ_{lv} of 72 mJ m^{-2}. Positive forces act away from the solid surface and negative forces act towards the solid surface.

From Eq. (14) it can be observed that thee situations can arise: $\varphi < \theta$, where the surface tension force is positive and directed away from the solid surface; $\varphi = \theta$, where the surface tension forces act parallel to the AWI; $\varphi > \theta$, where the surface tension force is negative and causes attachment. Figure 8 represents calculations of the surface tension force for different filling angles and contact angles. It can be seen that maximum surface tension detachment (positive) forces increase with particle hydrophobicity. Moreover, strongly hydrophilic particles only experience a positive surface tension force when a low filling angle is present. These calculations are valid for both drainage and imbibitions events.

However, in contrast to Figures 6, the AWI approaches the attached particle from an angle. It was found by Gao et al., (2006) that the water films in their pore scale experiments did not expand gradually, but were abruptly eliminated as an unsaturated pore was filled almost instantaneously with water. Figure 9 gives a more realistic visualization of the position of the AWI's with respect to a particle during a drainage situation. Depending on the hydrophobicity of the substratum, the AWI approaches the colloid at a different angle (α). Figure 9a represents drainage on a hydrophilic substratum and Figure 9b represents drainage on a hydrophobic substratum. For these cases, the maximum value for F_γ can be obtained by differentiating Eq. (14) with respect to φ, giving the result $\varphi=\theta/2$. The component of this force in the vertical direction is $F_\gamma \cos \alpha$. (Leenaars and O'Brien, 1989). Substituting this into Eq. (14), the maximum surface tension detachment forces for a hydrophilic and hydrophobic substratum are, respectively (Boks et al., 2008):

$$F_\gamma^{\max} = 2\pi R_p \gamma_{lv} \sin^2\left(\frac{\theta}{2}\right)\cos(\alpha) \qquad for\ \alpha < 90^\circ \qquad (15)$$

$$F_\gamma^{\max} = -2\pi R_p \gamma_{lv} \sin^2\left(\frac{\pi+\theta}{2}\right)\cos(\alpha) \qquad for\ \alpha > 90^\circ \qquad (16)$$

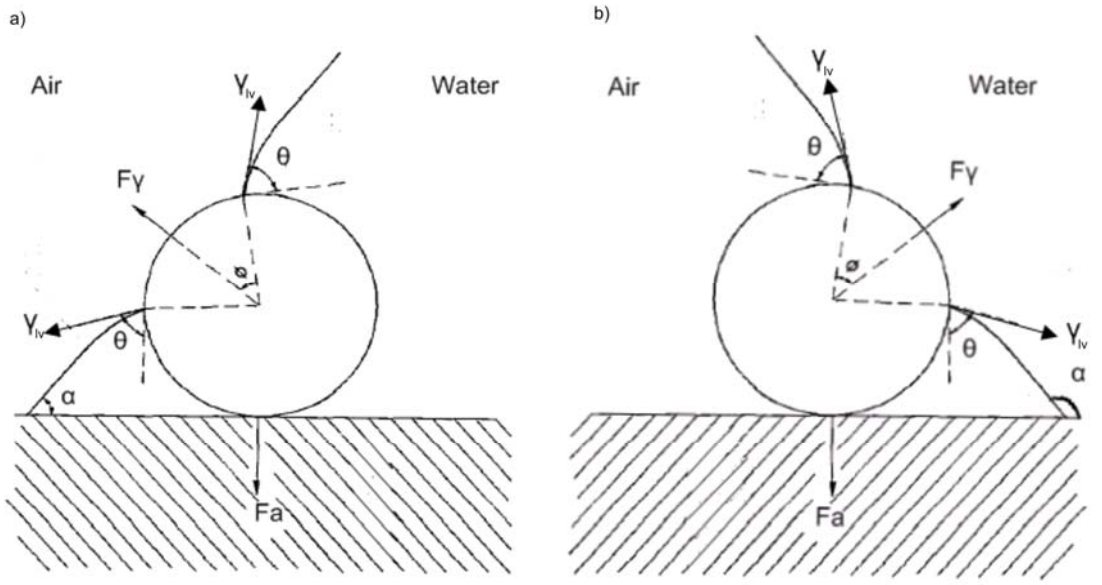

Fig. 9. Particle adhering to a substrate during the passage of an AWI. a: Hydrophilic substratum (Leenaars and O'Brien, 1989); b: Hydrophobic substratum

3.2. Parallel Plate Flow Chamber Experiments

On interface scale, several drainage experiments on the effect of a moving AWI on particle detachment have been done (Gómez-Suárez et al., 1999a, 1999b, 2001a, 2001b; Sharma et al., 2005; Boks et al., 2008). In these experiments, a parallel plate flow chamber was used through which an air bubble passed (Figure 10). During this process fluid drag forces are of less importance (Shang et al., 2008).

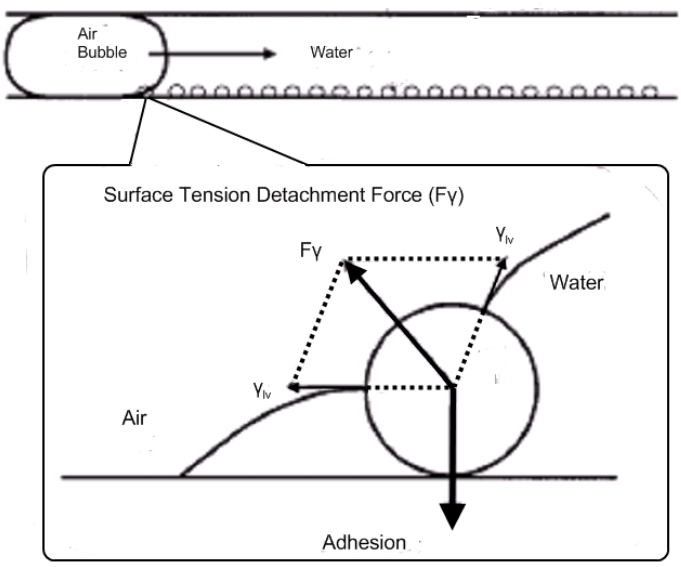

Fig.10. Surface tension detachment force, F_γ, experienced by a microbial cell due to the passing air-water interface (Sharma et al., 2005)

The probability of detachment from glass surfaces, P, can be expressed as (Schulze, 1992):

$$P = P_C \times P_A \times P_S \qquad (17)$$

where P_C is the bubble-particle collision probability, P_A is the bubble-particle attachment probability and P_S is the probability that the particle bubble aggregate will remain stable during transport away from the collector surface. In these parallel plate flow chamber experiments, if the air bubble fully spans the width of the flow chamber, the collision probability approaches unity. Visualization of colloids attached to the AWI shows that even if there are repulsive energies between colloids, detachment from the AWI is not very likely (Saiers et al., 2003). This indicates that P_S also approaches unity and that the detachment probability, therefore, mainly depends upon the bubble-particle attachment probability, P_A.

For the collision probability, P_C in Eq. (17) to be as high as possible, the liquid film between the colloid and the air-water interface should decrease until the following critical thickness is reached (Gómez-Súarez et al., 1990b):

$$h_{crit} = 23.3\left[\gamma_{lv}\left(1-\cos\theta_A\right)\right]^{0.16} \qquad (18)$$

where θ_A [º] is the advancing contact angle. Whether the critical thickness will be reached depends upon the air bubble velocity and the surface collector hydrophobicity. A lower air bubble velocity results in a longer time for drainage of the liquid film between the colloid and the air-water interface. This means the film thickness will reduce significantly. Therefore, higher detachment is observed at lower air bubble velocities. It should be kept in mind that these results are based on parallel plate flow chamber experiments through which air bubbles are pushed. During this process a certain velocity is given to the air bubble. A higher velocity may deform the bubble to a more oval, stretched shape. In this way the air bubble does not span the full width of the flow chamber and a significant liquid film between the air-water interface and the colloid remains and prevents collision (Figure 11).

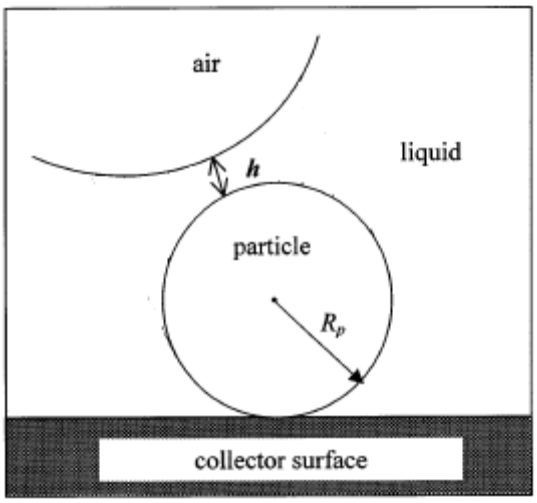

Fig. 11. Liquid film to be drained in order to form a three-phase contact between particle and air bubble and surface tension detachment forces to become operative (Gómez Súarez et al., 2001)

Collision probability does not only depend upon air bubble shape, but also on pore shape. Drainage of a parallel plate flow chamber by a full width spanning AWI means the water phase will be completely replaced by the air phase (Figure 10). Favorable attachment locations in saturated and unsaturated triangular pore space geometry are shown in Figure 1 and 4. After drainage, residual water will remain in the corners. Particles that are attached to the SWI in the low flow velocity corners will not collide with the moving AWI and remain attached. For Eq. (17) it means that the detachment probability could reach zero, because the collision probability, P_C, tends to zero. From this example, one can conclude that pore shape has an important effect on detachment probability.

4. Experimental Results from Drainage Events

4.1. Velocity of Air bubble

Several parallel-plate flow chamber experiments, with similar set-up as shown in Figure 10, are done by Gómez-Súarez (1999a/b; 2001a/b). Gómez-Suárez et al. (1999a) showed a linear increase in particle detachment from the collector surface with decreasing air bubble velocity. For the lowest velocity in their experiment, which was 2.37×10^{-3} $m \cdot s^{-1}$, a maximal particle detachment of 92% was found. This linear relationship holds regardless whether the collector surface is hydrophilic or hydrophobic, positively or negatively charged (Gómez-Suárez et al., 1999b) and regardless of the particle size (Gómez-Suárez et al., 2001a).

In line with the theory, experimental observations showed that detachment of polystyrene particles from *hydrophilic, positively-charged* glass is most sensitive to changes in air-bubble velocity, followed by *hydrophilic, negatively-charged*, and *hydrophobic, negatively-charged* collector surfaces, respectively (Gómez-Suárez et al., 1999b). This can be explained by the phenomena of spontaneous de-wetting of a hydrophobic surface (Gómez-Suárez et al., 1999b). The liquid film between the colloid and air-water interface reduces faster to its critical value on a hydrophobic collector surface than on a hydrophilic collector surface, because the initial film thickness is already smaller on a hydrophobic collector surface. Therefore, because the liquid film thickness decreases spontaneously on a hydrophobic collector surface, the critical film thickness is less sensitive for changes in air bubble velocity.

4.2. Interfacial Tension

With respect to interfacial tension it was found that particle detachment increased linearly with increasing interfacial tension (Figure 12; Gómez-Suárez et al., 1999a). The lower the air bubble velocity, the more sensitive the particle detachment is to an increase in interfacial tension. Similar to the effects in changes of air bubble velocity this linear relationship holds regardless of collector surface properties and particle size (Gómez-Suárez et al., 1999b and 2001a).

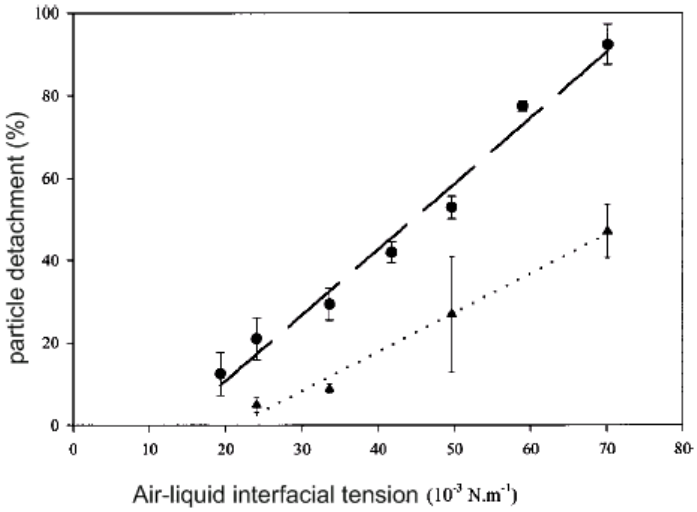

Fig. 12. Percentage of adhering particles removed from the substrate as a function of interfacial tension of different air bubble velocities of (●) 2.37 x 10^{-3} and (▲) 7.75 x 10^{-3} ms^{-1}. (Gómez-Súarez et al., 1999a)

In line with the theory, the experiments showed that detachment of colloids from a hydrophobic collector surface is less sensitive to changes in interfacial tension than detachment from a hydrophilic collector surface. This can be explained by the spontaneous de-wetting process as described in section 1.3.1. At odds with the theory, experiment results vary more for the less *hydrophilic, positively-charged* collector surface, than for the more *hydrophilic, negatively-charged* collector surface (Figure 13).

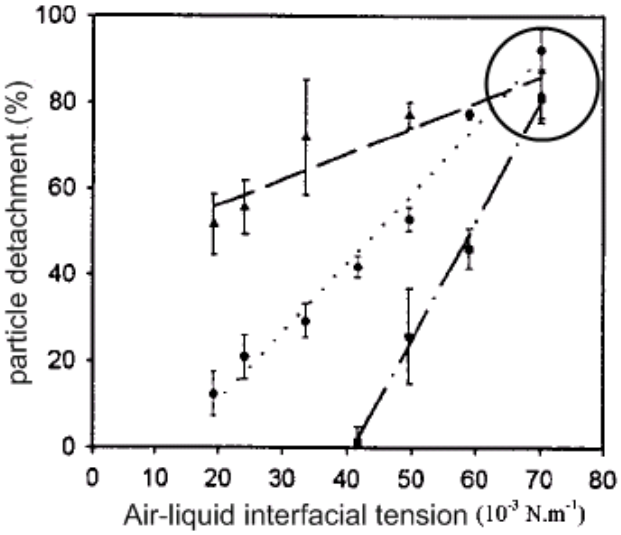

Fig. 13. Percentage of particles removed from (■) hydrophilic, positively, (▲) hydrophobic, negatively, and (●) hydrophilic, negatively charged collector surfaces as a function of the air-water interfacial tension (γ_{lv} for an air bubble velocity of 2.37 x 10^{-3} ms^{-1} (Gómez-Súarez et al., 1999b)

This phenomenon is also explained by Gómez-Suárez et al. (1999b) as a result of spontaneous de-wetting. However, the spontaneous thinning of the liquid film is greatest on the most hydrophobic collector surface and should be least on the most hydrophilic surface. The results in Figure 13 show a larger variability in detachment from the 'middle' hydrophilic surface than from the most hydrophilic surface. It seems more reasonable that this discrepancy is due to collector surface charge than hydrophobicity. This indicates that whenever the plates are negatively charged, colloid detachment from the most hydrophilic surface is most influenced. On the other hand, whenever a less

hydrophilic plate is positively charged it will be more influenced by changes in interfacial tension than the negatively charged more hydrophilic surface. In order to determine which of these factors is more dominant, additional research should be done with different surfaces. Furthermore, although it is not directly concluded in Gómez-Suárez et al. (1999b), the experiment results indicate that at low air bubble velocities and high interfacial tensions similar percentages of particles were detached, regardless of the type of collector surface (Figure 13, circle).

4.3. Particle Size

Regarding to particle size it was found that smaller polystyrene particles (diameter of 806 nm) are generally more readily detached from negatively charged surface collectors by a passing air-bubble than larger particles (diameter of 1400 nm) (Gómez-Suárez et al., 2001a). This is in contrast to Eq. (14), (15) and (16), which show that the theoretical surface tension detachment force increases with particle size. One explanation for this discrepancy may be the development of a particle-size-dependent resistive force during drainage of the liquid film, which prevents attachment to the AWI (Gómez-Suárez et al., 2001a). This resistive force can be expressed as (Bloom and Heindel., 1997):

$$F_T = \frac{6\pi\mu R_p^2 v_b}{hC_B} \qquad (19)$$

where μ [$ML^{-1}T^{-1}$] is the dynamic viscosity of the liquid, v_b [LT^{-1}] is the velocity of the air bubble, h [L] is the liquid film thickness and C_B [-] is the degree of retardation of the air bubble due to coverage by detaching particles. For the flow chamber limited length, as employed in the experiments described in this paper, C_B=1.

4.4. Particle Hydrophobicity

Sharma et al. (2005) showed that when an AWI passed by, 70 to 80% of the *S. oralis* cells and 85 to 98% of the *A. naeslundii* cells were detached from a hydrophilic glass plate (Table 1). It was found in theoretical calculations that surface tension detachment forces of a moving AWI during imbibition (Figure 8) were much larger for hydrophobic particles than for hydrophilic particles. At short separation distances, the adhesion forces for hydrophilic and hydrophobic particles were equal (Sharma et al., 2008). Thus, attached hydrophilic and hydrophobic particles experience equal adhesion forces, but higher detachment forces for hydrophobic particles than for hydrophilic particles. If this theory is applied to a drainage situation, the strength of the surface tension detachment force increases with hydrophobicity, which explains why the more hydrophobic *A. naeslundii* cells were more readily detached then the more hydrophilic *S. oralis* cells during the passage of a moving AWI.

5. Experimental Results from Imbibition Events

5.1. Detachment from SWI

A parallel plate flow chamber experiment as described in section 1.2 for drainage experiments was also used by Sharma et al. (2008) for an imbibition experiment. The effect of moving AWI's on the detachment of colloids deposited on an air-dried glass surface was examined. Results showed that hydrophobic particles were more readily detached from the glass collector surface than the hydrophilic particles. This result was in line with the theoretical surface tension detachment forces they had calculated with Eq. (14). The surface tension detachment force was approximately 10 times larger for hydrophobic than for hydrophilic particles (Figure 14a). The attachment force calculations were based upon the DLVO theory. Because the glass plate was initially air-dried, no capillary forces were taken into account.

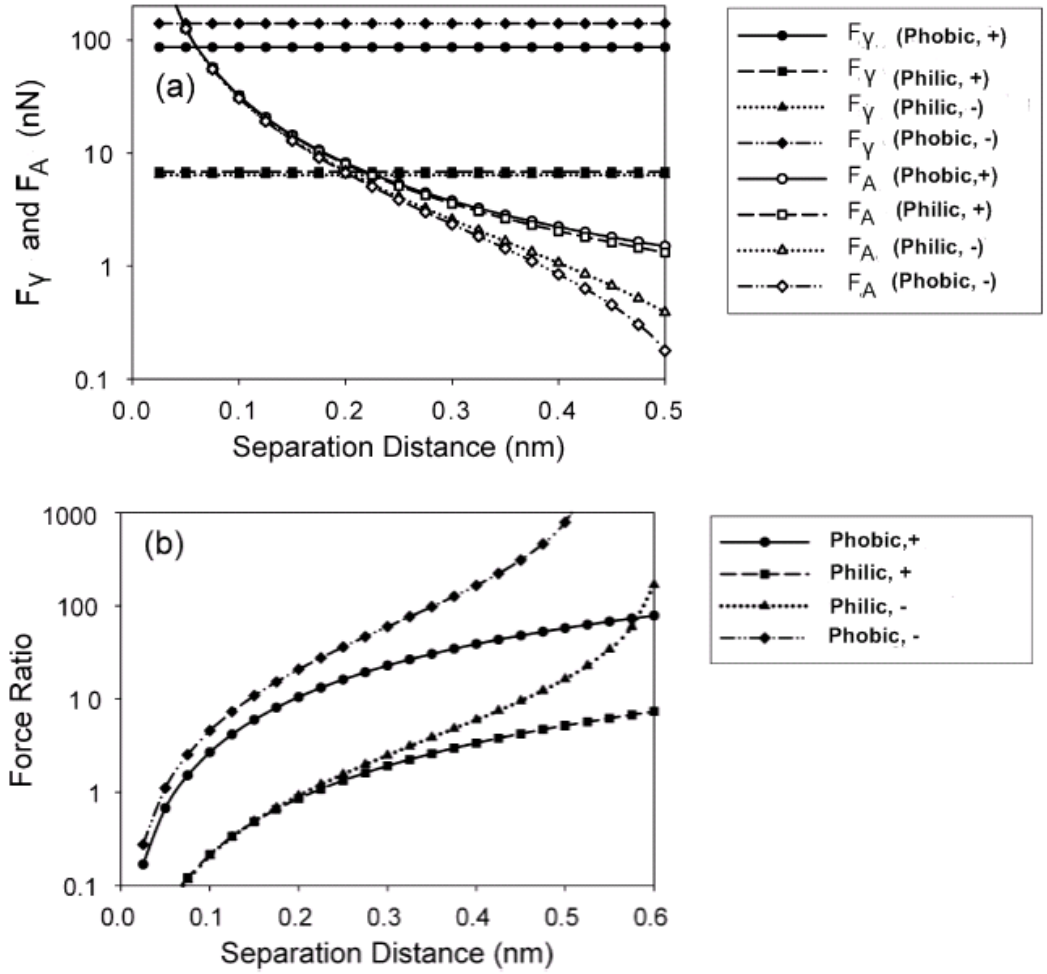

Fig. 14.(a) Detachment and attachment forces of hydrophobic (Phobic), hydrophilic (Philic), negatively charged (-) and positively charged (+) particles and (b) ratio of detachment and attachment force, in relation to separation distance for the different particles (Sharma et al., 2008)

Figure 14b represents the ratio between detachment and attachment forces. The experimental results were in line with the theory that the sequence of particle detachment should have been according to detachment ratio: hydrophobic negatively charged > hydrophobic positively-charged > hydrophilic negatively-charged > hydrophilic positively-charged.

5.2. Detachment from AWI

In a visualization of colloid transport done by Sirivithayapakorn and Keller (2003), it was found that particles strongly attach to the AWI and do not detach as long as the AWI is present. During imbibition, two mobilization processes occur: (1) The AWI is no longer held in the pore space and attached colloids are moving along with it, (2) AWI's dissolve and the attached colloids tend to form clusters within water and move along with the flow. These findings were supported by theoretical calculations of the DLVO interaction energy between colloid-colloid and colloid-AWI. The calculation indicated that the attractive energy of the colloids at the AWI is larger than the energy barrier between colloids, and, therefore, cluster forming is likely to appear.

The extent of increase in particle concentration with the arrival of the wetting front depends strongly upon the initial water content (Sirivithayapakorn and Keller, 2004). The number of particles initially adsorbed to the AWI increases with decreasing water content, since the available AWI increases as the water content decreases. Therefore, the decrease in particle detachment due to imbibition as the initial water contents increases supports the idea that AWI plays a significant role in retaining particles.

5.3. Detachment from SWA contact line

Visualization techniques from Crist et al. (2005) showed that immobilization of hydrophilic particles due attachment to the SWA contact line is reversible. As soon as the water film expands because of an increase in flow rate, the adhered particles are swept away.

5.4. Immobile/ Mobile Water Zones

During transport through a porous medium, particles can enter the immobile water zones by diffusion and slow advection and spread throughout the zone (Gao et al., 2006). Immobile water zones are considered to be fragmented regions were pore water flow is imperceptible or at least much slower than the average pore water velocity. During an imbibition experiment done by Gao et al. (2006), as moisture content increased and immobile water was conversed to mobile water, particles were released from the immobile water zones. Interestingly, the timescale for particle mobilization during this immobile to mobile water conversion was on the order of seconds, which is hundreds of times faster than timescale for advective-diffusive transfer between immobile and mobile zones during the steady flow periods of the experiments.

Conclusion

Detachment of a particle from a solid surface during drainage or imbibition was found to be caused by surface tension detachment forces as a result of interfacial tension between air and water. Theoretical calculations have shown that surface tension detachment forces (range 10^{-6} – 10^{-8} N) are generally much higher than adhesion forces (range 10^{-15} - 10^{-16} N) (Gómez-Suárez et al., 2001b). The detachment probability depends on the AWI-particle collision probability, the AWI-particle attachment probability and the probability that the particle-AWI aggregate will remain stable during transport away from the collector surface. Since the detachment forces are much higher than the attachment forces and because it was found that attachment to an AWI is generally irreversible (Sirivithayapakorn and Keller, 2003), the AWI-particle collision probability seems to be the determining factor if detachment will occur. The collision probability approaches unity in a parallel plate flow chamber experiment with low air-bubble velocities. In other pore shapes, with corners of residual water, the collision probability decreases.

Experimental results have shown that the detachment probability varies with particle and collector surface properties. Factors, that play a role in detachment, are air-bubble velocity, strength of interfacial tension, particle and substratum hydrophobicity and particle size. Especially during an imbibition event detachment also depends on the location of attachment prior to imbibition. It seems that detachment from a SWI and a SWA contact line is more likely to occur than detachment from an AWI.

With respect to the column experiments that found an increase in particle concentration with the arrival of a drying or wetting front, this review shows that is probably due to moving AWI's. The appearance of a strong surface tension detachment force can sweep the particle from the solid surface. This may lead to a peak concentration in the groundwater, caused by transient flow conditions.

References

Bergendahl, J., and D. Grasso (1998) Colloid generation during batch leaching tests: Mechanics of disaggregation. Colloids Surf. A 135:193–205

Bergendahl, J., and D. Grasso (1999) Prediction of colloid detachment in a model porous media: Thermodynamics. AIChE J. 45:475–484

Bergendahl, J., and D. Grasso (2000) Prediction of colloid detachment in a model porous media: Hydrodynamics. Chem. Eng. Sci. 55:1523–1532

Bloom, F., and T.J. Heindel (1997) A theoretical Model of Flotation Deinking Efficiency. J Colloid Interface Sci. 190:182-197

Boks, N.P., W. Norde, H.C. van der Mei, H.J. Busscher (2008) Forces involved in bacterial adhesion to hydrophilic and hydrophobic surfaces. Microbiology 154:3122-3133

Bradford, S.A., S.R. Yates, M. Bettahar, J. Šimůnek (2002) Physical factors affecting the transport and fate of colloids in saturated porous media. Water Resour. Res. 38(12):1327, doi:10.1029/2002WR001340

Bradford, S.A., J. Šimůnek, M. Bettahar, M.Th . van Genuchten, S.R. Yates (2006a) Significance of straining in colloid deposition: Evidence and implications. Water Resour. Res. 42:W12S15, doi:10.1029/2005WR004791

Bradford, S.A., J. Šimůnek, S.L. Walker (2006b) Transport and straining of *E. coli* O157:H7 in saturated porous media. Water Resour. Res. 42:W12S12, doi:10.1029/2005WR004805

Bradford, S. A., and S. Torkzaban (2008) Colloid transport and Retention in Unsaturated Porous MEdia: A review of Interface-, Collector-, and Pore-Scale Processes and Models. Vadose Zone Journal 7: 667-681

Burdick, G.M., N.S. Berman, S.P. Beaudoin (2005) Hydrodynamic Particle Removal from Surfaces. Thin Solid Films 488:116-123

Chateau, X., P. Moucheront, O. Pitois (2002) Micromechanisms of unsaturated granular media. J. Eng. Mech. 128:856-863

Chu, Y., Y. Jin, M. Flury, M.V. Yates (2001) Mechanisms of virus removal during transport in unsaturated porous media. Water Resources Research Vol. 37, NO. 2:253-263

Crist, J. T., Y. Zevi, J. F. McCarthy, J. A. Troop, T.S. Steenhuis (2005) Transport and retention mechanisms of colloids in partially saturated porous media, Vadose Zone J. 4:184–195

Derjaguin, B.V., and L.D. Landau (1941) Theory of the stability of strongly charged lyophobic sols and of the adhesion of strongly charged particles in solutions of electrolytes. Acta Physicochim. URSS 14:733-762

Ducker, W.A., Z. Xu, J.N. Israelachvili (1994) Measurements of Hydrophobic and DLVO Forces in Bubble-Surface Interactions in Aqueous Solutions. Langmuir 10:3279-3289

Gao, B., J. E. Saiers, J. N. Ryan (2006) Pore-scale mechanisms of colloid deposition and mobilization during steady and transient flow through unsaturated granular media. Water Resour. Res. 42, W01410, doi:10.1029/2005WR004233

Goldman, A.J., R.G. Cox, H. Brenner (1967) Slow viscous motion of a sphere parallel to a plane wall: I. Motion through a quiescent fluid. Chem. Eng. Sci. 22:637–651

Gómez-Suárez, C., J. Noordmans, H.C. van der Mei, H.J. Busscher (1999a) Removal of Colloidal Particles from Quartz Collector Surfaces as Stimulated by the Passage of Liquid-Air Interfaces. Langmuir, 15:5123-5127

Gómez-Suárez, C., J. Noordmans, H.C. van der Mei, H.J. Busscher (1999b) Detachment of colloidal particles from collector surfaces with different electrostatic charge and hydrophobicity by attachment to air bubbles in a parallel plat flow chamber. Phys. Chem. Chem. Phys. 1:4423-4427

Gómez-Suárez, C., H.C. van der Mei, H. J. Busscher (2001a) Air bubble induced detachment of polystyrene particles with different sizes from collector surfaces in a parallel flow plate flow chamber. Phys. and Engineering Aspects 186:211-219
Gómez-Suárez, C., H.J. Busscher, H.C. van der Mei (2001b) Analysis of Bacterial Detachment from Substratum Surfaces by the Passage of Air-Liquid Interfaces. Appl. and Envir. Microbiology 2531-2537
Grasso, D., K. Subramaniam, M. Butkus, K. Strevett, and J. Bergendahl (2002) A review of non-DLVO interactions in environmental colloidal systems. Rev. Environ. Sci. Biotechnol. 1:17–38
Hamaker, H. C. (1937) The London-van der Waals attraction between spherical particles. Physica 4:1058-1072
Hogg, R., D.S. Cahn, T.W. Healy, and D.W. Fuerstenau (1966) Diffusional mixing in an ideal system. Chem. Eng. Sci. 21:1025–1038
Israelachvili, J.N. (1992) Intermolecular and surface forces. 2nd ed. Academic Press, London
Jin, Y., Y.Chu, Y. Li (2000) Virus removal and transport in saturated and unsaturated sand columns. J. Contam. Hydrol. 43:111 –128
Johnson, W.P., X. Li, and G. Yal. (2007) Colloid retention in porous media: Mechanistic confirmation of wedging and retention in zones of flow stagnation. Environ. Sci. Technol. 41:1279–1287
Keller, A. A., and S. Sirivithayapakorn (2004) Transport of colloids in unsaturated porous media: Explaining large-scale behavior based on pore-scale mechanisms. Water Resour. Res. 40 W12403, doi:10.1029/2004WR003315
Leenaars, A. F. M. and S.B.G. O'Brien (1989) Particle removal from silicon substrates using surface-tension forces. Philips J Res 44:183–209
Liu, Y., and J. H. Tay (2002) The essential role of hydrodynamic shear forces in the formation of biofilm and granular sludge. Water Res**.** 36:1653–1665
O'Neill, M.N. (1968) A sphere in contact with a plane wall in a slow linear shear flow. Chem. Eng. Sci. 23:1293–1298
Norde, W, and J. Lyklema (1989) Protein adsorption and bacterial adhesion to solid-surfaces-A colloid-chemical approach. Colloids Surf 38:1-13
Powelson, D. K., A.L. Mills (2001) Transport of Escherichia in Sand Columns with Constant and Changing Water Contents. J. Environ. Qual. 30:238-245
Ramachandran, V., and H.S. Fogler (1999) Plugging by hydrodynamic bridging during flow of stable colloidal particles within cylindrical pores. J. Fluid Mech. 385:129–156
Saiers, J.E., G.M. Hornberger, D.B. Gower, J.S. Herman (2003) The role of moving air-water interfaces in colloid mobilization within the vadose zone. Geophys. Res. Lett. 30, No 21
Schäfer, A., H. Harms, A.J.B. Zehnder (1998) Bacterial accumulation at the air-water interface. Environ. Sci. Technol. 32:3704-3712
Schijven, J. F. and S. M. Hassanizadeh (2000) Removal of Viruses by Soil Passage: Overview of Modeling, Processes, and Parameters. Critical Reviews in Environmental Science and Technology 30:1,49-127
Schulze, H. J., Adv. Colloid Interface Sci., (1992) 40, 283 in Gómez-Suárez et al., 1999b.
Shang, J., M. Flury, G. Chen, J. Zhuang (2008) Impact of flow rate, water content, and capillary forces on in situ colloid mobilization during infiltration in unsaturated sediments. Water Resour. Res. 44
Sharma, P., M. Flury, J. Zhou (2008) Detachment of colloids from a solid surface by a moving air-water interface. Journal of Colloid and Interface Science 326:143-150
Sharma, P. K., M.J. Gibcus, H.C. van der Mei, H.J. Busscher (2005) Influence of Fluid Shear and Microbubbles on Bacterial Detachment from a Surface. Applied and Environmental Microbiology 3668-3673

Sirivithayapakorn, S., and A. Keller (2003) Transport of colloids in unsaturated porous media: a pore-scale observation of processes during the dissolution of the air-water interface. *Water Resour. Res.*, *39*, 1346, doi: 10.1029/2003WR002487
Soltani, M., and G. Ahmadi (1994) On particle adhesion and removal mechanics in turbulent flows. J. Adhes. Sci. Technol. 8:763–785
Thompson, S. S., M. Flury, M. V. Yates, and W. A. Jury (1998) Role of the air-water-solid interface in bacteriophage sorption experiments. Appl. Environ. Microbiol. 64:304–309
Thompson, S.S., and M.V. Yates (1999) Bacteriophage inactivation at the air-water-solid interface in dynamic batch systems, Appl. Environ. Microbiol. 65(3):1186–1190
Torkzaban, S., S.M. Hassanizadeh, J.F. Schijven, A.M. de Bruin, A.M. de Roda Husman (2006a) Virus Transport in Saturated and Unsaturated Sand Columns. Vadose Zone Journals 5:877-885
Torkzaban, S., S.M. Hassanizadeh, J.F. Schijven, H.H.J.L. van den Berg (2006b) Role of air-water interfaces on retention of viruses under unsaturated conditions. Water Resources Research Vol 42, W12S14, doi:10.1029/2006WR004904
Veerapaneni, S., J. Wan, and T.K. Tokunaga (2000) Motion of particles in film flow. Environ. Sci. Technol. 34:2465–24
Verwey, E.J.W., and J.Th .G. Overbeek (1948) Theory of the stability of lyophobic colloids. Elsevier, Amsterdam
Yoon, R., D.H. Flinn, Y.I. Rabinovich (1997) Hydrophobic interactions between dissimilar surfaces. Journ. of Coll. and Interf. Sci. 185:363-370
Zhang, L., L. Ren, S. Hartland (1996) More convenient and suitable methods for sphere tensiometry, J. Colloid Interface Sci. 180:493–503

Part 2: Model

Supervisors:

Prof. dr. ir. S. Majid Hassanizadeh
Professor of Hydrogeology
Department of Earth Sciences
Faculty of Geosciences
Utrecht University, The Netherlands

Drs. Amir Raoof
Department of Earth Sciences
Faculty of Geosciences
Utrecht University, The Netherlands

Table of Contents

List of Symbols

α	empirical parameter [-]
C	concentration in water [pfu L^{-3}]
D	dispersion coefficient [L^2T^{-1}]
h	water pressure head [L]
k_{att}	attachment coefficient [T^{-1}]
k_{det}	detachment coefficient [T^{-1}]
k_{det}^{i}	detachment coefficient [T^{-1}]
K	hydraulic conductivity [L^2T^{-1}]
K_s	saturated hydraulic conductivity [L^2T^{-1}]
L	bottom of column [L]
m	empirical parameters [-]
μ_l	inactivation rate liquid [T^{-1}]
μ_s	inactivation rate solid [T^{-1}]
n	porosity [-]
N_0	inward flux [LT^{-1}]
N_C	number of compartments [-]
N_d	empirical coefficient [-]
p	empirical parameter[-]
q	Darcy velocity [LT^{-1}]
ρ_b	bulk density [ML^{-3}]
S	adsorbed concentration [pfu M^{-1}]
S_e	effective water content [-]
t	time
θ	water content [-]
θ_r	residual water content [-]
θ_s	saturated water content [-]
v	pore water velocity [LT^{-1}]
x	spatial coordinate in column [L]

Introduction

As mentioned before, the efficiency of RBF depends on hydrological factors, such as fluctuations in water saturation. Because the maximum concentration of viruses allowed in drinking water (VROM, 2001) is below detection limits, a model can provide an estimation of required filtration distance. To be able to provide a prediction of the virus concentration at the extraction well, the concept of detachment under transient flow conditions requires further research. The aim of this paper was to fully model the breakthrough curve of a drainage experiment done by Torkzaban et al. (2006). Previous modeling of virus detachment under transient flow regimes was done by Cheng and Saiers (2009). Their detachment concept was used in this paper to model the experiment.

The first chapter gives a description of one of the experiments done by Torkzaban et al (2006) which is used in this study to compare modeling results with. In the second chapter, the modeling computer programs and methods are described. The third and fourth chapters provide the concepts for the saturated and drainage models. A separate section, 4.2.2., describes the conceptual model of Cheng and Saiers (2009). In chapter five the results of the modeling are presented. At last, the modeling results are discussed and conclusions are drawn.

1. Previous Research

1.1. Experiment Selection

Torkzaban et al. (2006) have done several column experiments to virus transport under various water contents and solution chemistries. Their objective was to study the interaction of viruses with the SWI's and the AWI's under a variety of conditions. From that study, one experiment is selected for this research to compare modeling results with. The experiment of specific interest is labeled LpHi100, of which bacteriophage φX174 is observed explicitly. The experimental measurements are shown in Figure 1. Experimental conditions of this column experiment as well as modeling parameters can be found in Table 1.

Table 1. Experimental conditions of column experiment.

Experiment	LpHi100
pH	7
Ionic Strength (mM)	19
Saturation (%)	100
Pore Water Velocity (cm min^{-1})	0.68
Dispersivity (cm)	0.060
Seeding Duration (p.v.)	4.2
Porosity (-)	0.27
Column Length (cm)	23
Attachment Rate (min^{-1})	8.2 x 10^{-3}
Detachment Rate (min^{-1})	1.4 x 10^{-3}
Inactivation Rates (min^{-1})	1.3 x 10^{-5}
Bulk density (kg cm^{-3})	1650
Saturated Hydraulic Conductivity (cm min^{-1})	1.13
Residual Water Content (-)	0.078

Arguments for selecting experiment LpHi100 were:
(1) An increase in breakthrough concentration was seen for bacteriophage φX174 with the arrival of the drying front. Torkzaban et al. (2006) were able to model virus transport prior to drainage, during the steady state saturated flow. This study aims to model the rising tail of the breakthrough curve as well.
(2) Bacteriohage φX174 could be modeled by a one-site kinetic model in the saturated and unsaturated experiments. This indicated that attachment to stagnant AWI's (during unsaturated flow) was insignificant. During drainage, both stagnant and moving AWI's occur. Since the main point of interest is the role of moving AWI's, the influence of stagnant AWI's could be eliminated by selecting bacteriophage φX174.
(3) Prior to drainage the saturation of the column is 100%. Therefore, the bacteriophages could initially only be attached to the SWI's. Argument (2) actually already states that attachment of bacteriophage φX174 to the stagnant AWI's is negligible; however, any uncertainties according to this assumption can be removed by argument (3).

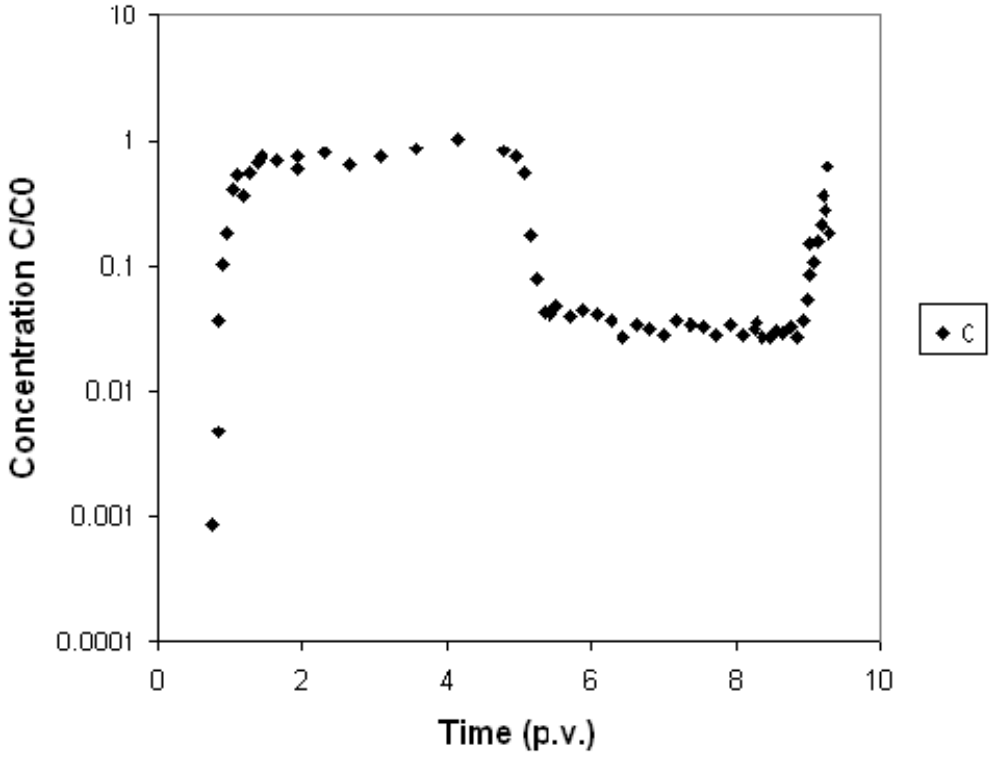

Figure 1. Measured (symbols) breakthrough curve of φX174 at pH 7 and ionic strength 19 mM in Exp. LpHi100; C/Co on log scale (Torkzaban et al., 2006).

1.2. Column Set-up and Measurements

Torkzaban et al. (2006) followed the procedure of Robinson and Friedman (2001) to produce a homogeneous wet-packed sand column. A cylindrical PVC column with an internal diameter of 10 cm and length of 23 cm was used. Sand with a median grain size (d_{50}) of 140 μm and uniformity (d_{60}/d_{10}) of 1.6 was used as the porous medium. A

detailed description of how the sand was treated can be found in Torkzaban et al. (2006). To establish a water flow velocity in the saturated column that was comparable with the velocities in the unsaturated columns, a hydraulic gradient was applied. Then, during 4.2 pore volumes the virus suspension was added to the system. One pore volume is equal to approximately 2040 seconds, which makes the pulse input time equal to 8571 seconds. The total time of the experiment lasted 9.3 pore volumes, i.e. 18970 seconds. Effluent samples were taken from the outlet of the column at regular intervals and analyzed for virus concentrations.
Using the Hydrus 1D software package (Simunek et al., 1998), the experimental results were modeled. Model parameter average pore water velocity was measured directly from the water flux and water content. The liquid inactivation rate was measured in a batch experiment and assumed to be equal to the soil inactivation rate (Schijven and Hassanizadeh, 2000). The dispersivity was calculated from inverse modeling of the breakthrough data of the tracer. The attachment and detachment rates were obtained from fitting the model to the experimental results (Table 1).

2. Saturated Flow and Transport

2.1. Water Flow Equations

The equation for one-dimensional saturated flow is given by Darcy's law:

$$q = -K_s\left(\frac{dH}{dx}\right) \tag{1}$$

where q [LT^{-1}] is the water flux, H [L] is the hydraulic head, and K_s [LT^{-1}] is the saturated hydraulic conductivity. The corresponding boundary conditions are:

$$K_s\left(\frac{dH}{dx}\right) = N_0 \qquad at \quad x = 0 \tag{2a}$$

$$h = h_0 \qquad at \quad x = L \tag{2b}$$

where N_0 [LT^{-1}] is the inward flux into the domain normal to the boundary, h [L] is the water pressure head. At the bottom of the column (x=L) a constant pressure head (h_0) was applied. The value for h_0 was chosen such that a saturated flow velocity of N_0 was established.

2.2. Virus Transport Equations

The equation for virus transport through the saturated column is given by a one-dimensional advection-dispersion-adsorption-inactivation equation:

$$\frac{\partial C}{\partial t} + \frac{\rho_b}{n}\frac{\partial S}{\partial t} = \frac{\partial}{\partial x}\left(D\frac{\partial C}{\partial x}\right) - v\frac{\partial C}{\partial x} - \mu_l C - \mu_s\frac{\rho_b}{n}S \tag{3}$$

where C [pfu L^{-3}] is the number of viruses in water, S [pfu M^{-1}] is the number of adsorbed viruses per unit mass of soil, ρ_b [ML^{-3}] is the bulk density, D [L^2T^{-1}] is dispersion coefficient, v [LT^{-1}] is the pore water velocity, n [-] is the porosity, and μ_s [T^{-1}] and μ_l [T^{-1}] are the inactivation rate coefficients at the solid grains and in the water, respectively. The according equation for adsorption of viruses to the SWI is (Schijven and Hassanizadeh, 2000):

$$\frac{\partial S}{\partial t} = \frac{n}{\rho_b}k_{att}C - k_{\det}S - \mu_s S \tag{4}$$

where k_{att} [T^{-1}] and k_{det} [T^{-1}] are the attachment and detachment rate coefficients, respectively. The upper boundary condition for the water concentration is:

$$C(0,t) = C_0 \qquad 0 < t < t_{pulse} \qquad (5a)$$

$$C(0,t) = 0 \qquad t_{pulse} < t < t_{end} \qquad (5b)$$

where t_{pulse} represents the final time of the pulse input and t_{end} represents the final time of the experiment.
The boundary condition at the bottom of the column is:

$$\left(nD \frac{\partial C}{\partial x} \right) = 0 \qquad t \geq 0 \qquad (6)$$

Initial conditions for the water concentration and adsorbed concentration are:

$$C(x,0) = 0 \qquad x \geq 0 \qquad (7a)$$

$$S(x,0) = 0 \qquad x \geq 0 \qquad (7b)$$

3. Drainage and Transport

3.1. Water Flow Equations

The equation to simulate the drainage of the column was governed by the Richard's equation:

$$\frac{\partial \theta}{\partial t} = \frac{\partial}{\partial x}\left[K(\theta)\left(\frac{\partial h}{\partial x} + 1 \right) \right] \qquad (8)$$

where θ [-] is the water content and K [LT^{-1}] the unsaturated conductivity. To describe the nonlinear relationship between θ and h the Van Genuchten expression was used (Van Genuchten, 1980):

$$\theta(h) = \begin{cases} \theta_r + \dfrac{\theta_s - \theta_r}{(1 + |\alpha h|^p)^m} & h < 0 \\ \theta_s & h \geq 0 \end{cases} \qquad (9a)$$

$$K(h) = K_s S_e^l \left[1 - \left(1 - S_e^{\frac{1}{m}} \right)^m \right]^2 \qquad (9b)$$

where θ_r [-] is the residual water content, S_e [-] is the effective water content, α [L^{-1}], p [-] and m [-] are empirical parameters with m=1-1/p. The corresponding boundary conditions for the drainage model are:

$$K\left(\frac{\partial h}{\partial x} + 1 \right) = 0 \qquad at \quad x = 0 \qquad (10a)$$

$$h = 0 \qquad at \quad x = L \qquad (10b)$$

The initial condition for the pressure head distribution was derived from the steady state distribution in the saturated flow model. The initial pressure head distribution in the column was expressed as:

$$h(x, 0) = \frac{-h_0}{L} x \qquad (11)$$

3.2. Virus Transport Equations

The one-dimensional equations for virus transport and adsorption during drainage are:

$$\frac{\partial \theta C}{\partial t} + \rho_b \frac{\partial S}{\partial t} = \frac{\partial}{\partial x}\left(\theta D \frac{\partial C}{\partial x} \right) - \frac{\partial qC}{\partial x} - \mu_l \theta C - \mu_s \rho_b S \qquad (12)$$

$$\frac{\partial S}{\partial t} = \frac{\theta}{\rho_b} k_{att} C - k_{\det} S - \mu_s S \qquad (13)$$

The upper boundary condition is:

$$\left(\theta D \frac{\partial C}{\partial x} - qC \right) = 0 \qquad t \geq 0 \qquad (14)$$

The lower boundary condition is:

$$\left(\theta D \frac{\partial C}{\partial x} \right) = 0 \qquad t \geq 0 \qquad (15)$$

The initial conditions for the water concentration and adsorbed concentration profiles were obtained from the distribution at the final time of the saturated experiment. The distributions were plotted against the depth of the column. The trend line was calculated and used as initial distribution when drainage started. The initial conditions for the water concentration and the adsorbed concentration are:

$$C(x,0) = C_0(x) \qquad (16a)$$

$$S(x,0) = S_0(x) \qquad (16b)$$

3.3. Simulating Transient Kinetic Adsorption

3.3.1. Constant Detachment Rate

The detachment rate, k_{det}, as shown in Eq.(4) and Eq.(13) was initially modeled as a constant value. Fitting of the experiment results as was done by Torkzaban et al. (2006), provided a detachment constant with which the experimental results of virus transport during saturated flow were modeled well. However, as mentioned before, changing water contents can increase virus detachment significantly. In order to model virus transport during drainage, at first, the detachment constant was increased until the rising tail of Figure 1 could be fitted satisfactorily. However, a constant detachment rate does not describe the actual physical process occurring during drainage and could not give a satisfactory result. The next step was to extend the model by incorporating a variable detachment rate as proposed in a previous drainage experiment done by Cheng and Saiers (2009).

3.3.2. Variable Detachment Rate

Since it has been found that it is actually the moving AWI's (e.g. Powelson and Mills, 2001; Saiers et al., 2003) that cause additional virus detachment during drainage, Cheng and Saiers (2009) developed a detachment concept that depends upon changes in water content. They assumed that colloid mobilization occurs from pores that undergo snap-off, which means from pores that empty during drainage. An increase in capillary pressure, or

decrease in water pressure, forces air to enter the pore. The heterogeneity in pore sizes leads to a distribution of snap-off pressures which are ordered in a number of compartments. Once a compartment gets activated because its critical snap-off pressure is reached, particles are removed from the soil grains. The total adsorbed concentration is a summation of the adsorbed concentrations in the different compartments:

$$\frac{\partial S}{\partial t} = \sum_{i=1}^{Nc} \frac{\partial S_i}{\partial t} \qquad (17)$$

where N_C is the number of compartments and S_i is the adsorbed concentration associated with the *i*th compartment.

The concept of Cheng and Saiers (2009) was slightly adjusted in this study. They assumed that there was no detachment prior to drainage and the only detachment was caused by pore snap-off. In this paper, a constant detachment rate was considered for saturated pores and additional detachment occurs from pores that undergo snap-off. Based on these assumptions, the temporal change in adsorbed virus concentrations can be expressed as:

$$\frac{\partial S_i}{\partial t} = \frac{\theta}{\rho_b}\frac{1}{N_C} k_{att} C - k_{\det} S_i - \mu_s S_i - k_{\det}^{i} S_i \qquad (18)$$

where $k_{det}^{\ i}$ [T^{-1}] is the detachment rate coefficient, representing detachment from the solid grains induced by a passing AWI. The relationship for $k_{det}^{\ i}$ that applies during drainage is (Cheng and Saiers, 2009):

$$k_{\det}^{i} = 0 \qquad for\ h > h_{si} \qquad (19a)$$

$$k_{\det}^{i} = N_d \left| \frac{\partial \theta}{\partial t} \right| \qquad for\ h \le h_{si} \qquad (19b)$$

where θ_s [-] is the saturated water content, N_d [-] is an empirical coefficient that quantifies the kinetics of virus mobilization during a drainage event, and h_{si} is the critical snap-off pressure for compartment *i*. From Eq. (19a) and (19b) it can be observed that detachment takes place when the water pressure has declined to the critical water pressure head. Once air enters a pore, detachment occurs as long as flow is locally non-steady (i.e., $\partial\theta/\partial t \neq 0$).

The critical snap-off water pressure heads for the different compartments can be obtained from the cumulative density of snap off pressures:

$$F(h_s) = \bar{\theta} = \frac{\theta - \theta_r}{\theta_s - \theta_r} = \frac{1}{\left(1 + |\alpha h|^{p}\right)^{m}} \qquad (20)$$

where $F(h_s)$ is the cumulative density of h_s and $\bar{\theta}$ is the dimensionless moisture content. The continuous piecewise distribution of h_s needs to be discretized into a number of compartments, N_C, in order to provide a numerical solution that is compatible with

Eq.(18) (Saiers and Lenhart, 2003). $F(h_s)$ is divided into N_C evenly spaced values between zero and unity, which all provide one snap-off pressure for each compartment.
The initial conditions for the adsorbed virus concentrations in the different compartments are assumed to be uniformly divided across all N_C compartments (Saiers and Lenhart, 2003):

$$S_i(x,0) = \frac{1}{Nc} S(x,0) \qquad (21)$$

3.4. Numerical Modeling

3.4.1. Modeling Methods

The governing equations and according boundary and initial conditions as described in the previous sections were solved numerically using the 1D COMSOL Multiphysics 3.5a software package. In the Earth Science Module the fluid flow was simulated using Darcy's law and Richard's equation. Virus transport simulations were done by solving a convection- diffusion equation and partial differential equations in the COMSOL Multiphysics Module. In a coupled model of COMSOL Multiphysics 3.5a and Matlab 7.8.0.(R2009a) the drainage simulations were fitted to the experimental data.
At first the breakthrough curve of the virus transport during saturated flow was modeled. This part of the breakthrough curve had already been modeled successfully by Torkzaban et al. (2006). A steady state saturated flow was created by a constant inward flux at the upper boundary and a constant pressure head at the lower boundary. Initially, the water concentration and adsorbed concentration in the column were zero. A pulse input was created by applying a Dirichlet boundary condition. At the lower boundary, an advective-flux boundary condition was applied, which neglects transport by dispersion perpendicular to the lower boundary.
Next, virus transport during drainage of the column was modeled. At this stage, there were three unknowns: the Van Genuchten parameters and the detachment rate. The parameter values were estimated by fitting the simulations to the experimental data. The optimization algorithm is explained in detail in the next section. As explained in the introduction, during drainage additional detachment of viruses from the solid grains due to passing AWI's has been observed in several column experiments. In this study two detachment rate scenarios were modeled. At first, the constant detachment rate was increased until the experimental results were fitted best. After that a detachment rate proposal from Cheng and Saiers (2009) was incorporated in the model. As initial conditions for the drainage model, the final distributions of the pressure head, water concentration and adsorbed concentration from the saturated simulation were used.

3.4.2. Genetic Algorithm

The main objective was to find a detachment constant that could satisfactorily simulate the experiment. There three unknown parameters were estimated simultaneously by finding the best fit of the simulations to the experimental data. The best fit was determined to be the minimum sum of squared residuals between measured and modeled

effluent virus concentrations that could be obtained. The optimal combination of parameters was found using the genetic algorithm. The genetic algorithm is a method for solving both constrained and unconstrained optimization problems, which is based on natural selection.

For this research, a constrained genetic algorithm was used, since it was known beforehand between which boundaries the parameters values had to be. The Van Genuchten parameters (Eq.(9a) and (9b)) for a sandy soil, with median grain size of 140 μm and uniformity of 1.6, are generally between 2 and 15 for p and between 14 m^{-1} and 35 m^{-1} for α. These constraints ensured that other solutions to the problem with unrealistic parameter values were not taken into account.

The genetic algorithm repeatedly modifies a population of individual solutions. For this case, one individual solution consisted of three parameters values. At each step, the genetic algorithm selects individual solutions at from the current population to be parents and uses them to produce the children for the next generation. A population size of 20 individual solutions and a repetition of 10 generations were used. This means that at every generation 20 solutions were generated of which the best were selected to be part of the next generation. Over successive generations, the population "evolves" toward an optimal solution.

The genetic algorithm uses three main types of rules at each step to create the next generation from the current population (Haupt and Haupt, 1998):

1) *Selection rules* select the individuals, called *parents*, that contribute to the population at the next generation. Only the best *parents* are retained for the next iteration of the algorithm.

2) *Crossover rules* combine two *parents* to form *children* for the next generation. There are variable reasonable ways to pair the *parents*. Also for this case, the *parents* are mostly chosen from the best solutions from the population.

3) *Mutation rules* apply random changes to individual *parents* to form *children*. This is done to avoid the problem of overly fast convergence into a local minimum. The routine is forced to explore other areas of the solution range by randomly introducing changes, or mutations, in some of the parameters.

In this research the default values of Matlab 7.8.0.(R2009a) were used for the three selection criteria.

4. Results

4.1. Saturated Flow and Transport

The simulated breakthrough curve of the virus concentration during saturated flow compared to the experimental results is presented in Figure 2. The concentration is normalized to C/C0 and plotted on a log scale. The symbols represent the experimental measurements taken at the outlet of the column and the line represents the simulated breakthrough concentration. The sum of squares is 0.59208. Apparently, the model could fit the experimental results satisfactorily, which means that the final concentration and pressure head distributions from the saturated model could be used as input for the drainage model.

The final water and adsorbed concentration profiles are shown in Figures 3 and 4. Also the adsorbed concentration plot is normalized to S/C0. A trend line has been added to the profiles in order to use the distributions as initial conditions for the drainage model. The constants for Eq. (16a) and (16b) can be observed from the equations on the charts; a = -0.1443, b = 0.0012, c = 0.00009, and d = 0.000142.

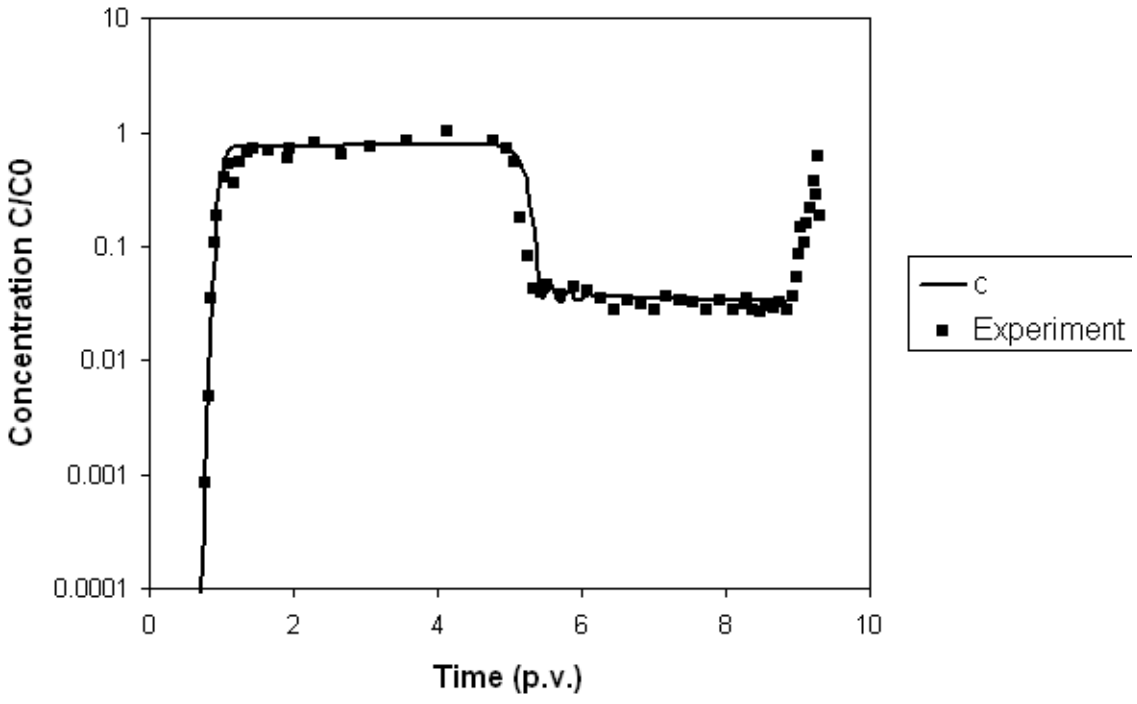

Figure 2. Measured (symbols) and fitted (line) virus concentration breakthrough curve on log scale.

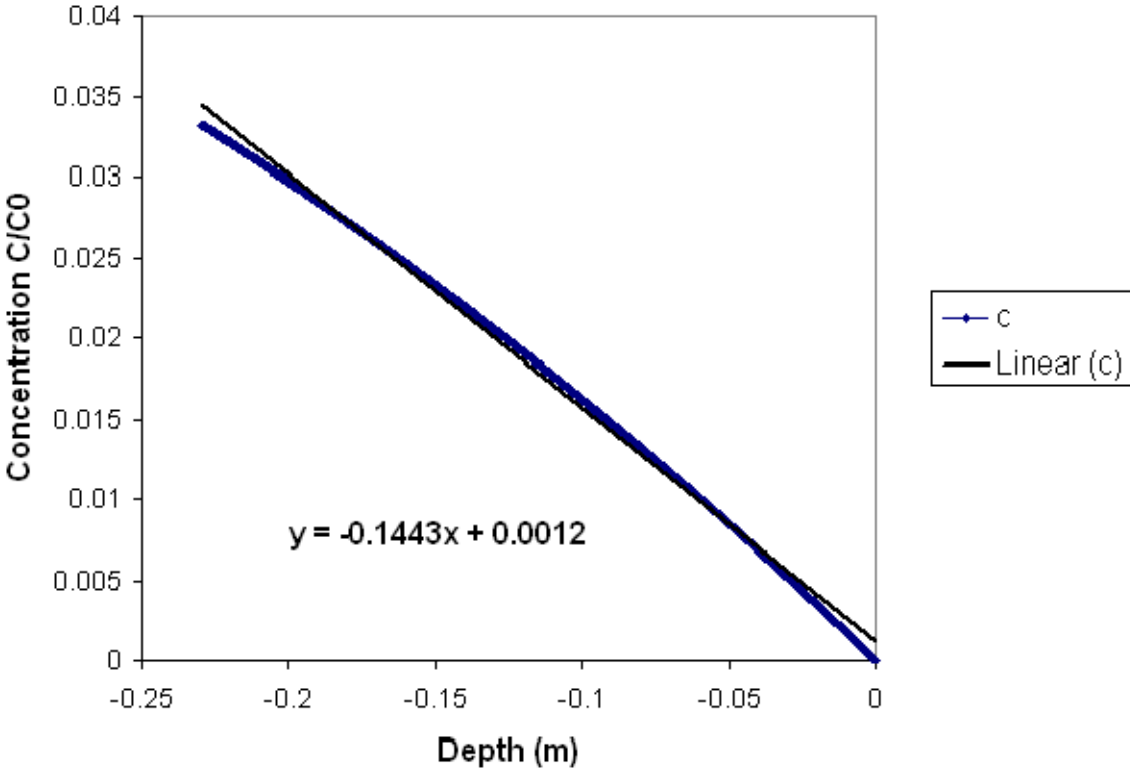

Figure 3. Virus concentration profile in water at time = 18000 s.

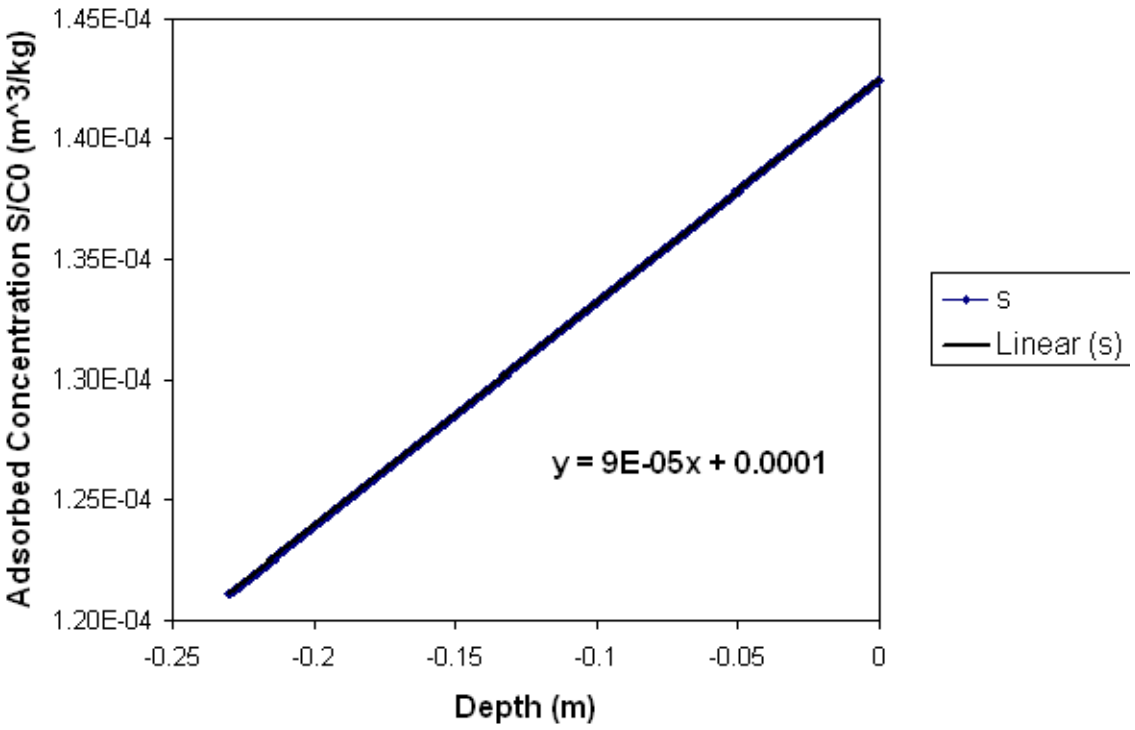

Figure 4. Adsorbed virus concentration profile at time = 18000 s

4.2. Drainage and Transport

4.2.1. Water Flow

As mentioned in the Methods and Materials, the Van Genuchten water retention parameters were estimated by fitting the concentration simulation to the experimental results. Therefore, there are three different Van Genuchten parameter sets for the three models. The parameters are shown in Table 2.

Table 2. Van Genuchten Parameters

Model	**p**	**α (m^{-1})**
Constant Detachment Rate	11.35	16.60
Variable Detachment Rate N_C = 5	10.58	28.46
Variable Detachment Rate N_C = 10	12.11	29.56

During drainage, the water pressure head declined as shown in Figure 5. In this plot, the Van Genuchten parameters from the transport model with a variable detachment rate and 5 compartments are used. The 5 critical snap-off pressures which are calculated with Eq.(20), are shown in Table 3. It can be observed from the graph that the column does not drain completely at all depths. For example, at z = -0.20 m, the last compartment (with the smallest pores) is not activated and therefore does not release additional viruses.

Table 3. Snap-off pressure heads

Compartment (*i*)	**Snap-off Pressure Head (h_{si})**
1	0
2	-0.0311
3	-0.0342
4	-0.037
5	-0.0408

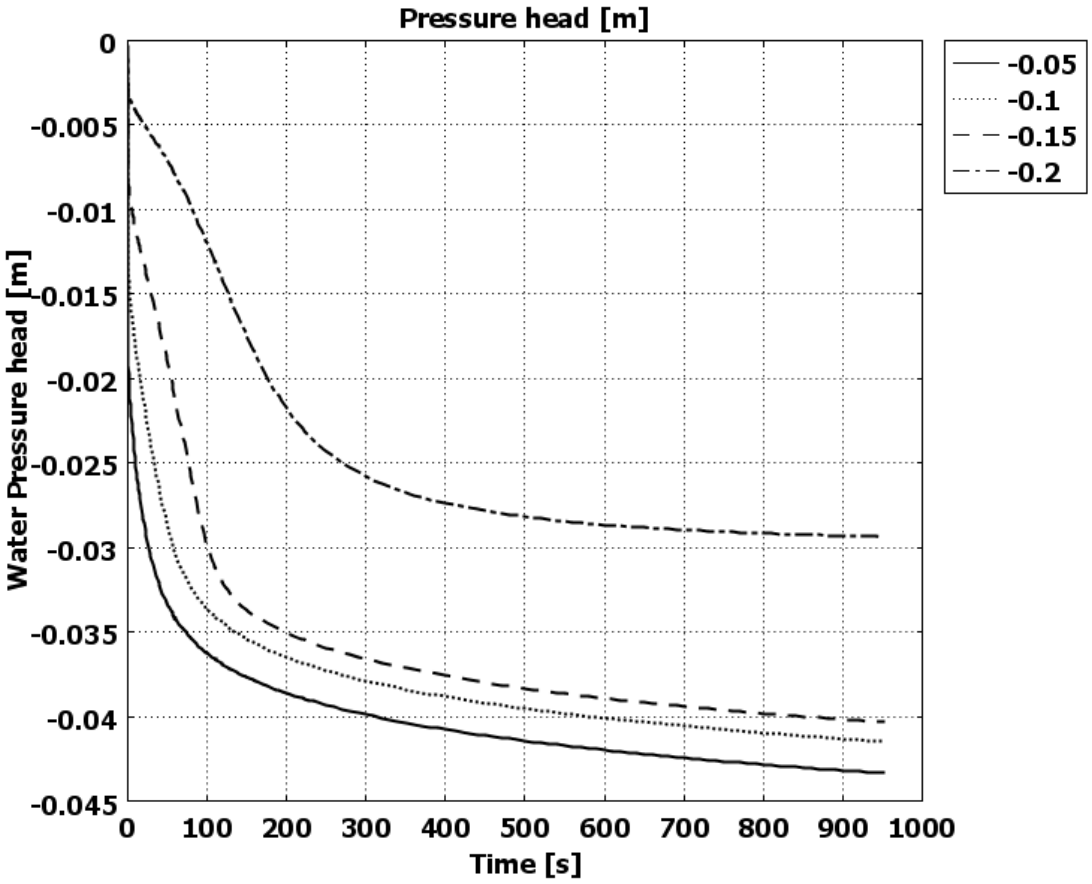

Figure 5. Water pressure head at z = -0.05, -0.1, -0.15 and -0.2.

4.2.2. Constant Detachment Rate

The simulation of the breakthrough curve during drainage with a constant detachment rate is shown in Figure 6. The detachment rate, k_{det}, has been increased from 0.000023 s^{-1} to 0.00070 s^{-1} in order to fit the experimental data. The sum of squares is 0.14127.

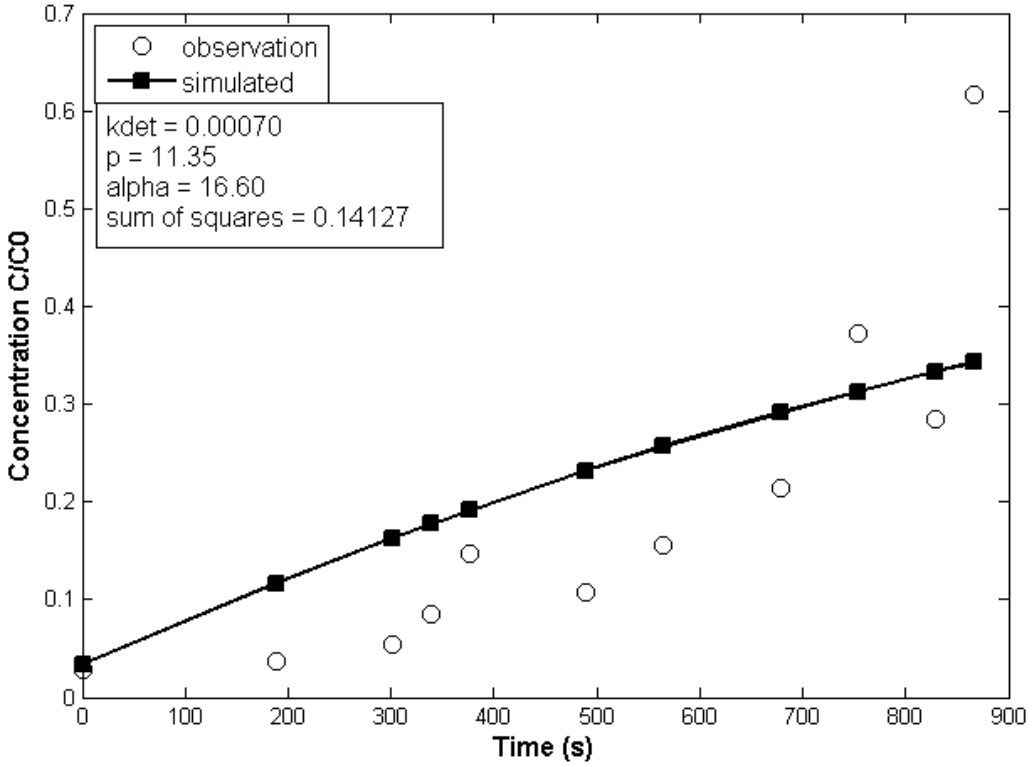

Figure 6. Drainage breakthrough curve with constant detachment rate

4.2.3. Variable Detachment Rate

Figure 7 shows the result of the drainage breakthrough curve with a detachment rate as proposed in Eq. (19a) and (19b), with 5 compartments. The optimal drainage constant, N_d, was found to be 52.53. Figure 8 shows the same result with 10 compartments, where N_d is 59.38. Both models fit the experimental data better than the model with a constant detachment rate (sums of squares are 0.082 and 0.074). The simulation with 10 compartments was more accurate than the simulation with five compartments.

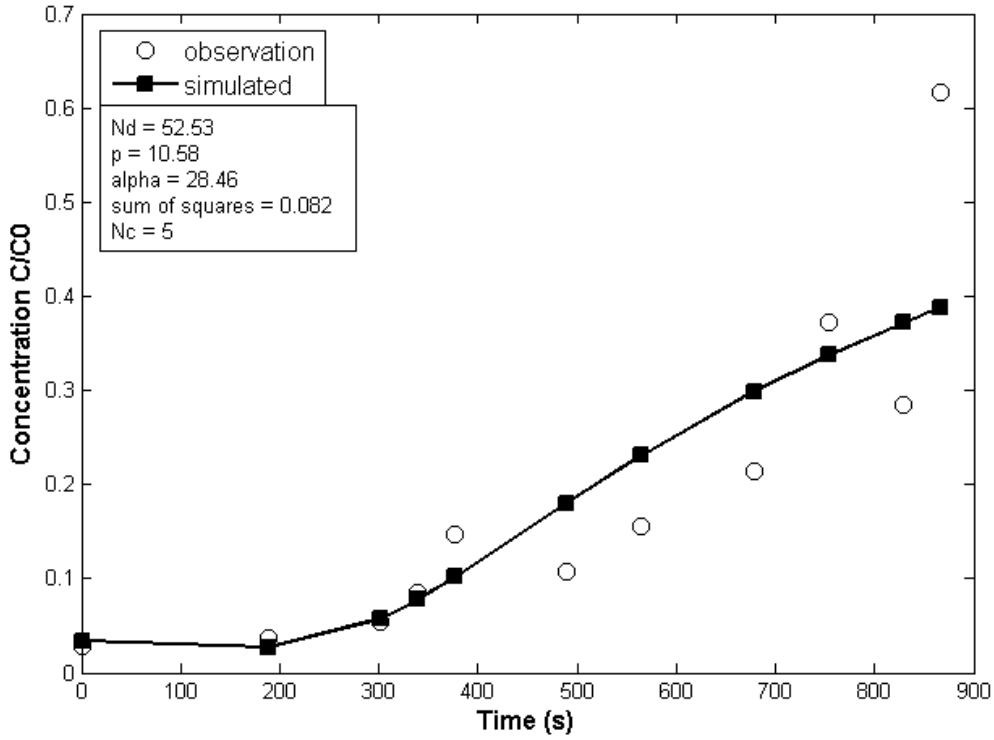

Figure 7. Drainage breakthrough curve with variable detachment rate.

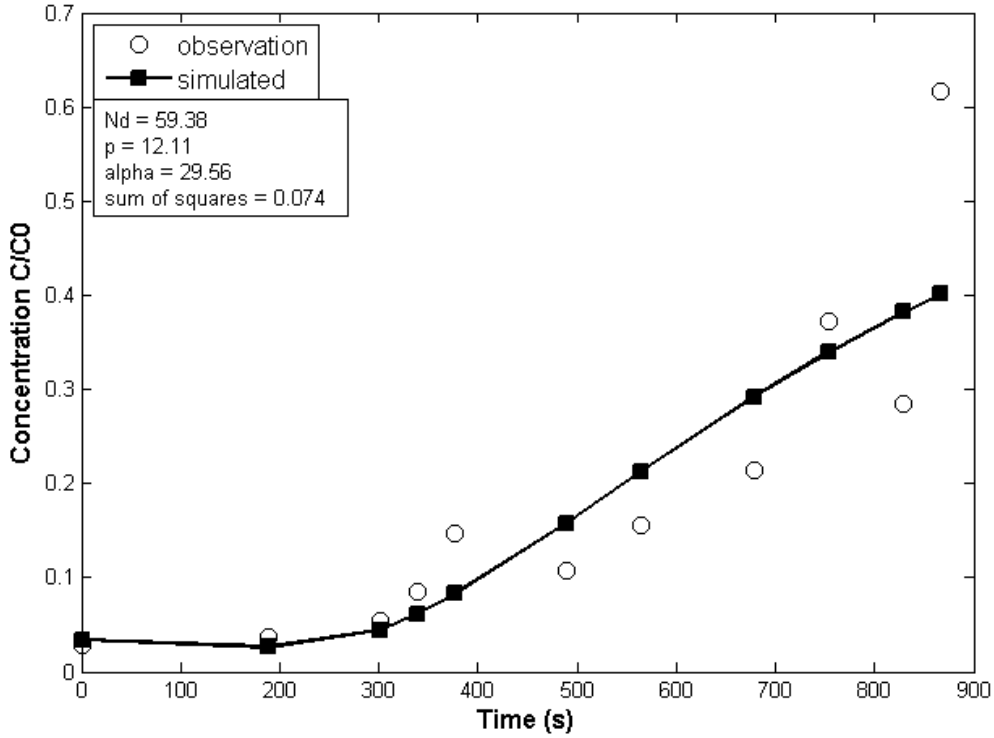

Figure 8. Drainge breakthrough curve with variabla detachment rate. Nc = 10

The factor that influences the variable detachment rate once it is activated, is the change in water content over time, $|\partial\theta/\partial t|$. Figure 9 shows the detachment rates of the five compartments at a depth of 0.1 meters. The vertical lines of the detachment rates show the exact time at which a new compartment is activated. Since all the detachment rates depend upon the same drainage constant, N_d, multiplied by the change in water content over time, the detachment rates will all follow the same curvature. The only difference between them is the time of activation. As was already seen from the pressure head distribution in Figure 5, not at all depths all five detachment rates were activated.

Finally, the results from the saturated model and the best fitting drainage simulation, the model with 10 compartments, are combined chronologically. The graph is shown in Figure 10. The visualization shows that the increase in concentration during drainage could be modeled satisfactorily with the detachment concept of Cheng and Saiers (2009).

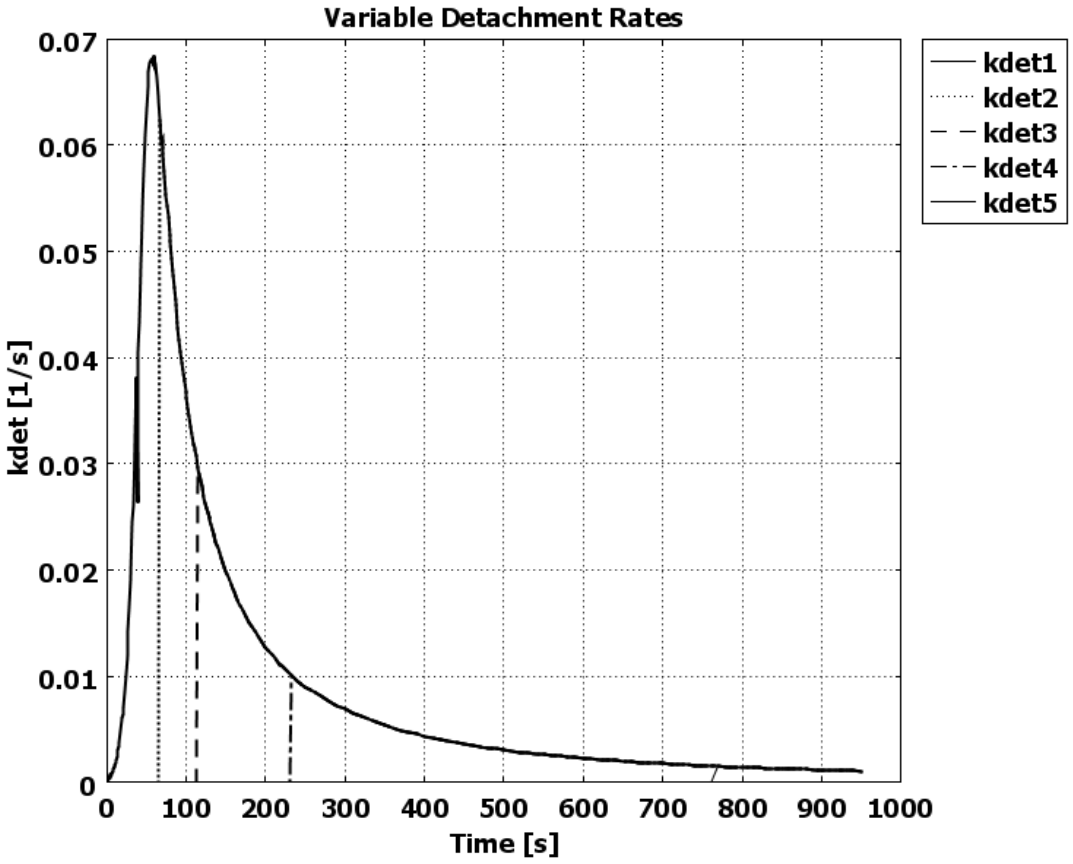

Figure 9. Variable detachment rates at z = -0.10 m

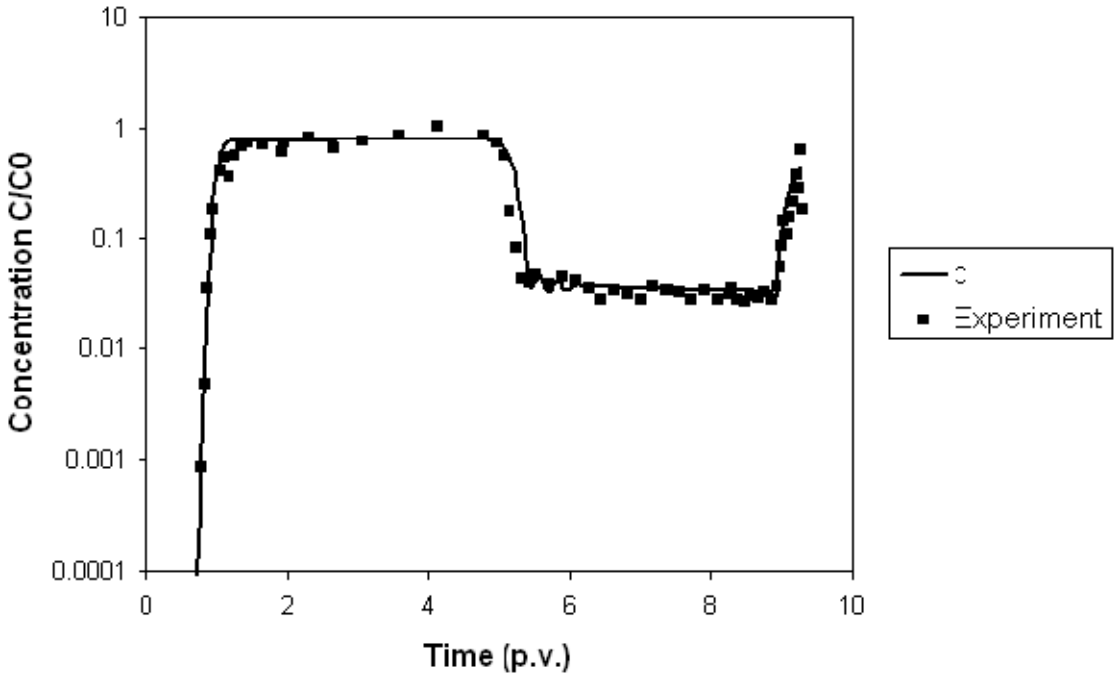

Figure 10. Complete simulation of the concentration breakthrough curve. The drainage part is modeled with a variable detachment rate and 10 compartments.

5. Discussion

As can be observed from the sums of squares of the three different models, the transport model with a variable detachment rate and 10 compartments simulates the experimental data set best. Visualization shows that the detachment process of viruses from SWI's during drainage can be described satisfactorily by a concept (Cheng and Saiers, 2009) that relates temporal changes in water content to detachment rates. The drainage constants, N_d, used in this study are approximately 5 to 10 times higher than the drainage constants found by Cheng and Saiers (2009).

The characteristic Van Genuchten water retention parameters were estimated by fitting the concentration simulations to the experimental data. Because the water flow model depended directly on the virus transport model, the three models have got a different set of Van Genuchten parameters to simulate the water flow during drainage. However, the Van Genuchten parameters are soil depended parameters and should therefore be equal for all simulations. Secondly, the virus transport model was now able to get optimized by optimizing the flow model. Therefore, with known Van Genuchten parameters, it could be suspected that the virus transport models would have provided a less good result. If only the drainage parameters, k_{det} and N_d, would have been optimized, the validity of the proposed detachment concepts would have been easier to test.

During drainage, the largest pores empty first. Therefore, the change in water content is highest in the beginning of the drainage and then slowly decreases. This can also be observed from Figure 9. The detachment rates depend linearly on the change in water content (Eq. 19b) and have the highest peak at the beginning of the drainage. The dependency of the detachment rate on the change is water content, is based upon the fact that it was found that moving air-water interfaces can mobilize colloids (e.g. Powelson and Mills, 2001; Saiers et al., 2003). A surface tension detachment force, which arises from the interfacial tension between air and water, can detach colloids when it exceeds the adhesion force (Leenaars and O'Brien, 1989). So, a change in water content leads to moving AWI's, which leads to additional detachment.

The simulation with 10 compartments provided a better result than the simulation with 5 compartments. As N_C increases, the discretized form of the distribution function (Eq.(20)) converges to the true, continuous form of the function (Hollenbeck et al., 1999). A higher non-uniformity of pore sizes requires a higher number of compartments. In this study, 10 compartments were considered sufficient, because the improvement from 5 to 10 compartments was small.

Conclusion

RBF is a potential and low-cost technology for extraction of cleaner and safer drinking water. Together with artificial recharge (AR), these forms of soil passage are applied to about 20% of the total drinking water supply. In other parts of the world, both techniques are expected to increasingly assist in solving the world water scarcity problem and in drinking water preparation. Because not every situation can be evaluated by measuring virus removal from groundwater, a model that reliably predicts removal over a certain time or distance is very useful. Steady state models on this subject might overestimate virus removal from groundwater, because they do not account for additional detachment of viruses caused by fluctuations in water content. In several soil column experiments, it was found that attached viruses can be remobilized by a passing drying front and can lead to a peak concentration in the water (e.g. Powelson and Mills, 2001; Saiers et al., 2003).

In this study, virus transport through a draining soil column was modeled and compared with experimental results from Torkzaban et al. (2006). The detachment of viruses from SWI's was modeled by two concepts and compared. One concept treats the detachment rate as a constant that increases when a transient flow condition is applied. The other concept is a detachment rate proposed by Cheng and Saiers (2009). This detachment rate is only activated when a pore gets drained and depends linearly on the temporal change in water content. Cheng and Saiers (2009) assumed that mobilization occurs from a pore that undergoes snap-off, or, in other words, a pore that empties during drainage. Non-uniformity in pore sizes gives a distribution of critical snap-off pressures. Comparison of the sum of squares of the models with respect to the experimental data showed that the concept of Cheng and Saiers (2009) could fit the data reasonably well and significantly better than the concept of the constant detachment rate.

Further research on this subject could be done on stabilizing the validity of the detachment concept of Cheng and Saiers (2009) by examining if the concept can be applied to a variety of one-dimensional column experiments. After that, the detachment concept could be introduced in two or three-dimensional problems on lab or field scale. With respect to RBF, it would be very useful to be able to model the influence of fluctuating water tables and infiltration patterns with a variable detachment rate. In any case, a detachment rate that automatically adjusts to changing flow patterns would be extremely important in reliable modeling of RBF.

References

Cheng, T and Saiers S E (2009) Mobilization and transport of in situ colloids during drainage and imbibition of partially saturated sediments. Water Resources Research Vol 45, W08414, doi:10.1029/2008WR007494, 2009

El-Farhan Y H, Denovio N M, Herman J S, and Hornberger G M (2000) Mobilization and transport of soil particles during infiltration experiments in an agricultural field. Shenandoah Valley, Virginia, Environ. Sci. Technol., 34, 3555– 3559

Haupt, R L, and S E Haupt (1998) Practical Genetic Algorithm. John Wiley & Sons, Inc. New York, USA. ISBN 0-471-18873-5

Hollenbeck, K. J., C. F. Harvey, R. Haggerty, and C. J. Werth (1999) A method for estimating distributions of mass transfer rate coefficients with application to purging and batch experiments, J. Contam. Hydrol., 37, 367–388, 1999.

Kaplan D I, Bertsch P M, Adriano D C, and Miller W P (1993) Soil-borne mobile colloids as influenced by water flow and organic carbon, Environ. Sci. Technol., 27, 1193– 1200

Leenaars, A. F. M. and S.B.G. O'Brien (1989) Particle removal from silicon substrates using surface-tension forces. Philips J Res 44:183–209

Powelson D K, Mills A L (2001) Transport of Escherichia in Sand Columns with Constant and Changing Water Contents. J. Environ. Qual. 30, 238-245

Robinson D A and Friedman S P (2001) The effect of particle size distribution on the effective dielectric permittivity of saturated granular media. Water Resour. Res. 37:33–40.

Ryan J N, Illangasekare T H, Litaor M I, Shannon R (1998) Particle and plutonium mobilization in macroporous soil during rainfall simulations. Environ. Sci. Techn.,32,476-482

Saiers, J. E., and J. J. Lenhart (2003) Colloid mobilization and transport within unsaturated porous media under transient-flow conditions, Water Resour. Res., 39(1), 1019, doi:10.1029/2002WR001370

Saiers J E, Hornberger G M, Gower D B, Herman J S (2003) The role of moving air-water interfaces in colloid mobilization within the vadose zone. Geophys. Res. Lett. 30, No 21

Schijven J F and Hassanizadeh S M (2000) Removal of viruses by soil passage: Overview of modelling, processes, and parameters. Crit. Rev. Environ. Sci. Technol. 30:49–127.

Simunek J, Sejna M, Genuchten M Th van (1998) The Hydrus- 1D software package for simulating the one-dimensional movement of water, heat, and multiple solutes in variably-saturated media. Version 2.0. USDA-ARS, U.S. Salinity Laboratory, Riverside, CA.

Torkzaban S, Hassanizadeh S M, Schijven J F, Bruin H A M de, Roda Husman A M de (2006) Virus Transport in Saturated and Unsaturated Sand Columns. Vadose Zone Journal 5:877-885.

Van Genuchten, M Th (1980) A closed-form equation for predicting the hydraulic conductivity of unsaturated soils. Soil Sci. Soc. Am. J. 44:892-898